Article

Cell Reports

HIV-1 Envelope Overcomes NLRP3-Mediated Inhibition of F-Actin Polymerization for Viral Entry

Graphical Abstract

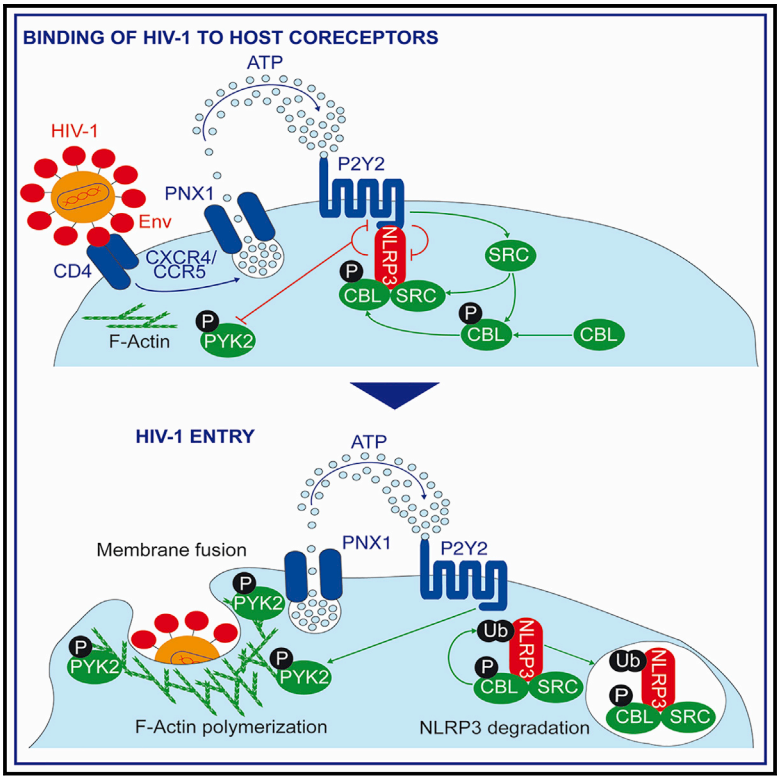

Highlights

- NLRP3 and P2Y2 interact and regulate susceptibility to HIV-1 infection
- NLRP3 is an intrinsic inhibitory factor for HIV-1 that represses F-actin remodeling
- HIV-1 Env binding to host receptors overcomes NLRP3 restriction by activating P2Y2
- P2Y2 activation leads to CBL-mediated NLRP3 degradation and favors viral entry

Authors

Audrey Paoletti, Awatef Allouch, Marina Caillet, ..., Marie-Lise Gougeon, Guido Kroemer, Jean-Luc Perfettini

Correspondence

perfettini@orange.fr

In Brief

Paoletti et al. identified a constitutive interaction between NLRP3 and P2Y2 that regulates HIV-1 entry into target cells. They revealed that NLRP3 represses viral entry by impairing F-actin reorganization. HIV-1 overcomes this host cellular resistance by inducing NLRP3 degradation through the activation of P2Y2-dependent signaling pathway.

Paoletti et al., 2019, Cell Reports *28*, 3381–3394
September 24, 2019 © 2019 The Author(s).
https://doi.org/10.1016/j.celrep.2019.02.095

CellPress

Cell Reports
Article

OPEN ACCESS
CellPress

HIV-1 Envelope Overcomes NLRP3-Mediated Inhibition of F-Actin Polymerization for Viral Entry

Audrey Paoletti,[1,2,3,4,24] Awatef Allouch,[1,2,3,4,24] Marina Caillet,[3,4,5] Hela Saïdi,[6] Frédéric Subra,[7] Roberta Nardacci,[8] Qiuji Wu,[1,2,3,4] Zeinaf Muradova,[1,2,3,4] Laurent Voisin,[1,2,3,4] Syed Qasim Raza,[1,2,3,4] Frédéric Law,[1,2,3,4] Maxime Thoreau,[1,2,3,4] Haithem Dakhli,[1,2,3,4] Olivier Delelis,[7] Béatrice Poirier-Beaudouin,[6] Nathalie Dereuddre-Bosquet,[9,10,11] Roger Le Grand,[9,10,11] Olivier Lambotte,[9,11,12] Asier Saez-Cirion,[13] Gianfranco Pancino,[13] David M. Ojcius,[14,15] Eric Solary,[16] Eric Deutsch,[2,3,4] Mauro Piacentini,[8,17] Marie-Lise Gougeon,[6] Guido Kroemer,[5,18,19,20,21,22,23,25] and Jean-Luc Perfettini[1,2,3,4,14,25,26,*]

[1]Cell Death and Aging Team, Gustave Roussy, 114 rue Edouard Vaillant, F-94805 Villejuif, France
[2]Laboratory of Molecular Radiotherapy, INSERM U1030, Gustave Roussy, 114 rue Edouard Vaillant, F-94805 Villejuif, France
[3]Gustave Roussy, 114 rue Edouard Vaillant, F-94805 Villejuif, France
[4]Université Paris Sud - Paris 11, 114 rue Edouard Vaillant, F-94805 Villejuif, France
[5]INSERM U848, Gustave Roussy, 114 rue Edouard Vaillant, F-94805 Villejuif, France
[6]Institut Pasteur, Antiviral Immunity, Biotherapy and Vaccine Unit, Infection and Epidemiology Department, 25 rue du Dr. Roux, F-75015 Paris, France
[7]CNRS UMR 8113 LBPA, Ecole Normale Supérieure de Cachan, 61 avenue du Président Wilson, F-94230 Cachan, France
[8]National Institute for Infectious Diseases "Lazzaro Spallanzani,", Via Portuense 292, 00149 Rome, Italy
[9]INSERM U1184, Center for Immunology of Viral Infections and Autoimmune Diseases, Fontenay-aux-Roses, France
[10]Université Paris Sud, UMR 1184, Fontenay-aux-Roses, France
[11]CEA, DSV/iMETI, Division of Immunology-Virology, IDMIT, Fontenay-aux-Roses, France
[12]APHP, Service de Médecine Interne – Immunologie Clinique, Hôpitaux Universitaires Paris Sud, F-94270 Le Kremlin-Bicêtre, France
[13]Unité HIV, Inflammation et Persistance, Institut Pasteur, 25 rue du Dr. Roux, F-75025 Paris, France
[14]Department of Biomedical Sciences, University of the Pacific, Arthur A. Dugoni School of Dentistry, 155 Fifth Street, San Francisco, CA 94103, USA
[15]Université Paris Diderot, Sorbonne Paris Cité, 75013 Paris, France
[16]INSERM U1009, Gustave Roussy, 114 rue Edouard Vaillant, F-94805 Villejuif, France
[17]Department of Biology, University of Rome "Tor Vergata,", Via della Ricerca Scientifica 1, 00133 Rome, Italy
[18]Metabolomics Platform, Gustave Roussy, 114 rue Edouard Vaillant, Villejuif, France
[19]Equipe 11 labellisée Ligue contre le Cancer, Centre de Recherche des Cordeliers, INSERM U1138, Paris, France
[20]Université Paris Descartes, Sorbonne Paris Cité, Paris, France
[21]Université Pierre et Marie Curie, Paris, France
[22]Pôle de Biologie, Hôpital Européen Georges Pompidou, AP-HP, Paris, France
[23]Karolinska Institute, Department of Women's and Children's Health, Karolinska University Hospital, Stockholm, Sweden
[24]These authors contributed equally
[25]Senior author
[26]Lead Contact
*Correspondence: perfettini@orange.fr
https://doi.org/10.1016/j.celrep.2019.02.095

SUMMARY

Purinergic receptors and nucleotide-binding domain leucine-rich repeat containing (NLR) proteins have been shown to control viral infection. Here, we show that the NLR family member NLRP3 and the purinergic receptor P2Y2 constitutively interact and regulate susceptibility to HIV-1 infection. We found that NLRP3 acts as an inhibitory factor of viral entry that represses F-actin remodeling. The binding of the HIV-1 envelope to its host cell receptors (CD4, CXCR4, and/or CCR5) overcomes this restriction by stimulating P2Y2. Once activated, P2Y2 enhances its interaction with NLRP3 and stimulates the recruitment of the E3 ubiquitin ligase CBL to NLRP3, ultimately leading to NLRP3 degradation. NLRP3 degradation is permissive for PYK2 phosphorylation (PYK2Y402*) and subsequent F-actin polymerization, which is required for the entry of HIV-1 into host cells. Taken together, our results uncover a mechanism by which HIV-1 overcomes NLRP3 restriction that appears essential for the accomplishment of the early steps of HIV-1 entry.

INTRODUCTION

Although the stimulation of innate immunity with vaccine adjuvants has been extensively and efficiently harnessed for the control of major infectious diseases (such as diphtheria, tetanus, and poliomyelitis), the cellular and molecular mechanisms that orchestrate immune responses against pathogens remain largely elusive, especially with respect to the early steps of infection. Immune sensing of HIV-1 by pathogen recognition receptors (PPRs) and cytoplasmic DNA sensors may partially hinder

This is an open access article under the CC BY-NC-ND license (http://creativecommons.org/licenses/by-nc-nd/4.0/).

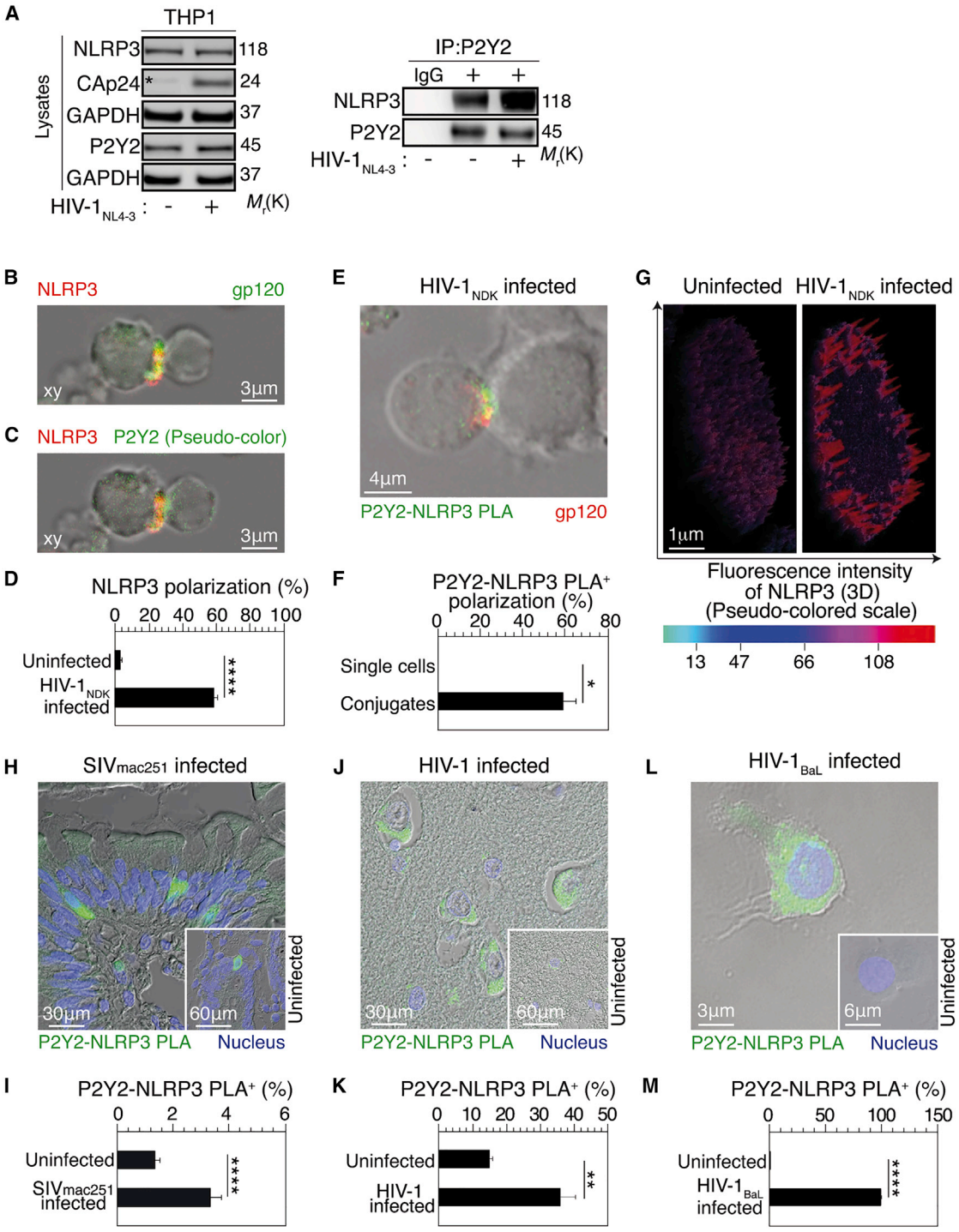

Figure 1. NLRP3 and P2Y2 Interaction Is Enhanced during HIV-1 and SIV Infections

(A) Immunoprecipitations were performed in THP1 cells after 3 h of X4-tropic HIV-1_{NL4-3} infection and analyzed by western blot. The asterisk indicates an unspecific band. Representative western blots of three independent experiments are shown. See also Figure S1A.

(B–D) Confocal microscopy images of NLRP3 (B and C), gp120 (B), and P2Y2 (C) polarizations during HIV-1-infected and uninfected lymphocyte interactions. Images are representative of three different donors. The frequency of NLRP3 polarization (D) is shown. Data are presented as means ± SEM, and significance is ****$p \leq 0.0001$ (n = 366 virological synapses from 3 independent experiments), unpaired Mann-Whitney test.

(legend continued on next page)

HIV-1 replication through the production of type-1 interferon (IFN) and the expression of restriction factors such as APOBEC3 cytidine desaminases, tetherin, and SAM domain and HD domain-containing protein 1 (SAMHD1) (Towers and Noursadeghi, 2014). Despite the beneficial impact of the cell-autonomous innate immune system on HIV-1 replication, innate signals, converging on the DNA sensing interferon gamma inducible 16 protein (IFI16) inflammasome, can contribute to chronic immune activation and eventually to pyroptosis of uninfected $CD4^+$ T cells, thereby enhancing disease progression (Doitsh et al., 2010, 2014; Monroe et al., 2014). Given the ambiguous effects of innate immune signals on HIV-1 replication and disease progression, further exploration of the innate signaling molecular pathways that govern HIV-1 infection is needed.

Most studies on HIV-1 infection have explored innate mechanisms acting before or after viral entry. Little is known about innate signaling pathways elicited during viral entry. We previously reported that purinergic receptors, which are membrane-anchored PPRs, promote the entry of HIV-1 into immune cells (Séror et al., 2011). The binding of HIV-1 envelope (Env) to its cellular receptors (CD4, CXCR4, and/or CCR5) causes the release of adenosine triphosphate (ATP) from host cells through the opening of pannexin-1 hemichannels (PNX1). Once released, extracellular ATP stimulates purinergic receptors (including the purinergic receptor P2Y2) and facilitates the membrane fusion process through the activation of the proline-rich tyrosine kinase 2 (PYK2) that is required for viral entry (Séror et al., 2011). The activation of the purinergic signaling pathway is indispensable for cell-free HIV-1 infection (Hazleton et al., 2012; Séror et al., 2011; Swartz et al., 2014), as well as for cell-to-cell transmission of the virus between infected lymphocytes and target cells, which is the most efficient route of HIV-1 spreading (Séror et al., 2011; Swartz et al., 2014). In this context, antagonists of purinergic receptors or pannexin-1 have emerged as a new class of HIV-1 microbicides (Séror et al., 2011).

Other PPRs, the NOD-like receptors (NLRs), have also been involved in the establishment of viral infection. Initially described as crucial for sensing and initiating host defense in viral infection through the formation of inflammasome (Chen and Ichinohe, 2015), NLRs (such as NLRX1) have recently been shown to be involved in the early innate response to simian immunodeficiency virus (SIV) infection and to contribute to viral replication by repressing the transcription of restriction factors (such as the interferon stimulated gene [ISG] 5, the myxovirus resistance 2 protein [MX2], and the tripartite motif-containing protein [TRIM] 5; Barouch et al., 2016). These results highlight the counterintuitive role of the inflammasome signaling, which indeed may facilitate (rather than repress) the early steps of HIV and SIV infections.

In this context and to further characterize cellular factors that may modulate P2Y2-dependent signaling during the early steps of HIV-1 infection, we studied the role of NLRs during viral infection. We identified the NACHT, LRR and PYD domains-containing protein 3 (NLRP3) as a P2Y2-interacting protein. Considering that NLRP3 and P2Y2 are endogenously expressed in $CD4^+$ T cells and cells from mononuclear phagocyte lineage (including monocytes and macrophages), we first studied the interaction between NLRP3 and P2Y2 during the cellular infection by HIV-1 and SIV. Then we characterized the biological consequences of the modulation of this interaction during the early steps of infection of macrophages, which are, together with T lymphocytes, the major target cells of HIV-1.

RESULTS

Enhancement of the Interaction between NLRP3 and P2Y2 during SIV and HIV Infection

Based on our previous work showing that the purinergic receptor P2Y2 contributes to the early steps of HIV-1 infection (Séror et al., 2011), we searched for potential P2Y2-interacting NLR proteins, identifying NLRP3 as an interactor of P2Y2 (Figure 1A). The endogenous NLRP3 and P2Y2 proteins co-immunoprecipitated in human THP1 monocytes (Figure 1A), indicating that both proteins constitutively interact. Of note, this interaction increased after 3 h of infection of human THP1 monocytes with CXCR4-tropic (X4-tropic) HIV-1_{NL4-3} (Figures 1A and S1A). We then studied the subcellular localization of NLRP3 during the early steps of HIV-1 infection obtained by co-culturing of uninfected peripheral blood lymphocytes (PBLs) with X4-tropic HIV-1_{NDK}-infected PBLs. NLRP3 polarized toward the contact sites formed between HIV-1_{NDK}-infected and uninfected host cells (Figures 1B and 1C). At these contact sites, NLRP3 colocalized with the glycoprotein gp120 (Figure 1B) and the purinergic receptor P2Y2 (Figure 1C). Thus, NLRP3 accumulated at the virological synapse that is formed between HIV-1_{NDK} -infected and uninfected PBLs (Figure 1D).

(E and F) PLA between P2Y2 and NLRP3 (E) and frequencies of positive signals (F) detected on interacting HIV-1-infected and uninfected lymphocytes are shown. The image is representative of three different donors. Data are presented as means ± SEM, and significance is *$p \leq 0.05$ (n = 29 virological synapses from three independent experiments), unpaired Mann-Whitney test.

(G) Fluorescence intensities of NLRP3 in HIV-1-infected and uninfected lymphocytes obtained from confocal microscopy are shown a three-dimensional (3D) Z-projection. Representative experiment of three different donors is shown.

(H and I) PLA between P2Y2 and NLRP3 (H) and frequencies of positive signals detected on ileum sections (I) obtained from SIV_{mac251}-infected and uninfected *Macaca fascicularis* are shown. Images are representative of four SIV_{mac251}-infected and three uninfected *Macaca fascicularis*. Data are presented as means ± SEM, and significance is ****$p \leq 0.0001$ (n = 3 uninfected, n = 4 uninfected), unpaired Mann-Whitney test.

(J and K) PLA between P2Y2 and NLRP3 (J) and frequencies of positive signals detected on brain autopsies (K) from HIV-1-infected and uninfected individuals are shown. Images are representative of nine HIV-1-infected and two uninfected donors. Data are presented as means ± SEM, and significance is **$p \leq 0.01$ (n = 2 uninfected, n = 9 infected), unpaired Mann-Whitney test.

(L and M) PLA between P2Y2 and NLRP3 (L) and frequencies of positive signals (M) detected during MDMs infection are shown. The image is representative of three different donors. Data are presented as means ± SEM, and significance is ****$p \leq 0.0001$ (n = 1,075 and 1,133 for uninfected and HIV-1_{BaL} infected MDMs, respectively), unpaired Mann-Whitney test.

See also Figure S1.

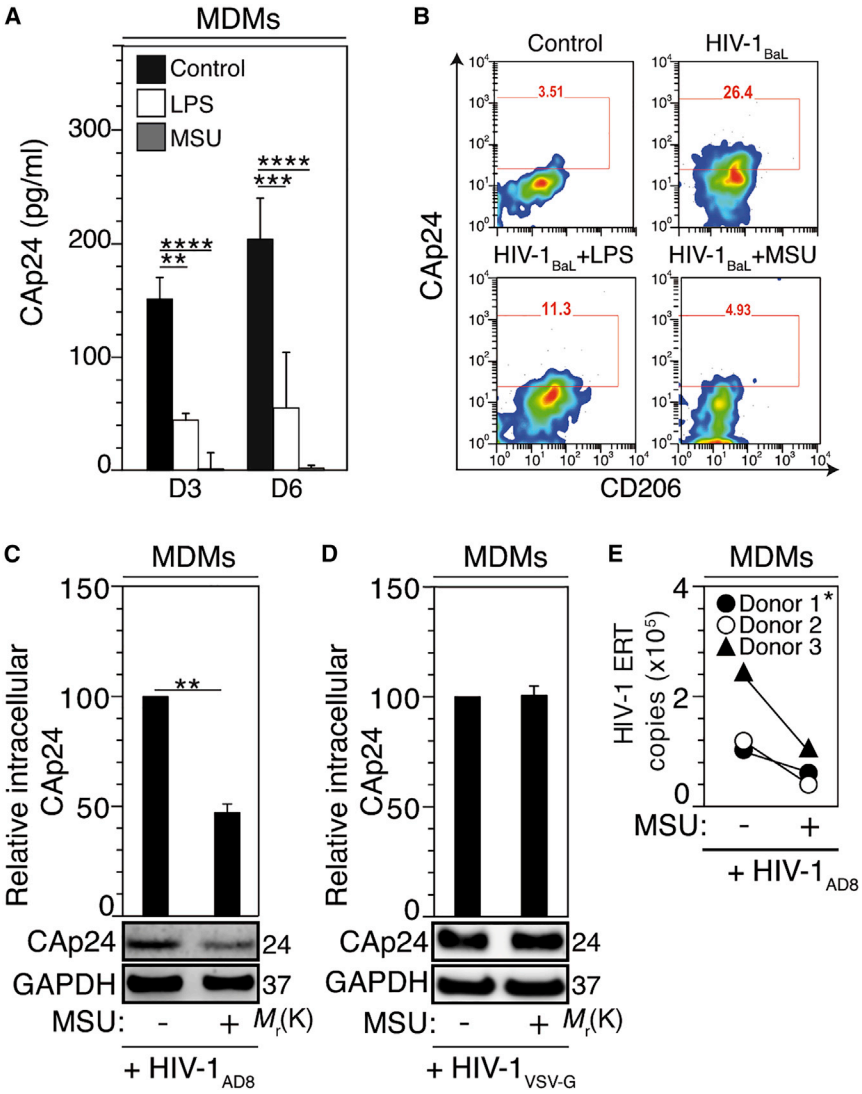

Figure 2. NLRP3 Inflammasome Activation Impairs HIV-1 Entry

(A and B) HIV-1 CAp24 content in cell supernatant analyzed by ELISA at 3 and 6 days (A) and intracellular CAp24 analyzed by flow cytometry at 6 days (B) after R5-tropic HIV-1_{BaL} infection of LPS- or MSU-treated MDMs. Data obtained from n = 3 independent experiments are presented in (A) as means ± SEM. Significance levels are $^{**}p \leq 0.01$, $^{***}p \leq 0.001$, and $^{****}p \leq 0.0001$, unpaired Mann-Whitney test. Representative flow cytometry analyses of three independent experiments are shown in (B).

(C and D) Intracellular CAp24 analyzed by western blot and the corresponding quantifications of control or MSU-treated MDMs that were infected for 6 h with R5-tropic HIV-1_{AD8} (C) or HIV-1_{VSV-G} (D). Representative western blots from three independent donors are shown. Data are obtained from three independent experiments presented as means ± SEM. Significance levels are $^{**}p \leq 0.01$ (n = 3 donors), unpaired t test.

(E) The number of copies of early reverse transcripts of HIV-1 (HIV-1 ERT) analyzed by qPCR in MDMs pretreated with 100 μM MSU for 18 h and infected for 6 h with HIV-1_{AD8} in the presence of MSU. ERT data were determined for three donors at 24 h after infection. Significance is $^{*}p \leq 0.05$ (n = 3 donors), Wilcoxon signed rank test.

See also Figures S2A, S2B, and S2C.

We determined the ability of NLRP3 to directly interact with P2Y2 by means of a proximity ligation assay (PLA). During the early steps of HIV-1 infection, the interaction between NLRP3 and P2Y2 mostly occurred at the contact sites between HIV-1_{NDK}-infected and uninfected T lymphocytes (Figures 1E and 1F). These results suggest that the interaction between NLRP3 and P2Y2 may regulate the viral entry into target cells. We also studied the subcellular localization of NLRP3 after chronic infection of PBLs with X4-tropic HIV-1_{NDK} for 72 h (Figures 1G and S1B–S1D) or that of monocyte-derived macrophages (MDMs) with R5-tropic HIV-1_{AD8} for 6 days (Figures S1E and S1F). While NLRP3 presented a diffuse cytosolic expression pattern in uninfected target cells, it aggregated in the cytoplasm and at the membrane of infected PBLs (Figures 1G and S1B–S1D) or MDMs (Figures S1E and S1F). Using PLA, we also evaluated the ability of NLRP3 to interact with P2Y2 during chronic infection and revealed that the interaction between NLRP3 and P2Y2 increased in chronically infected tissues (e.g., ileum [Figures 1H and 1I] and colon [Figures S1G and S1H] from SIV-1_{mac251}-infected non-human primate *Macaca fascicularis*, the frontal cortex from untreated HIV-1 carriers [as compared with uninfected controls; Figures 1J and 1K]), as well as in chronically infected PBLs (Figures S1I and S1J) or MDMs (Figures 1L and 1M). Altogether, these findings indicate that the interaction between NLRP3 and P2Y2 increased during acute and chronic steps of viral infection.

NLRP3 Inflammasome Activation Impairs HIV-1 Entry into Host Cells

To characterize the role of NLRP3-P2Y2 interaction and related signaling pathways during the early steps of HIV-1 infection, we first evaluated the possibility that the NLRP3 might affect viral replication through the formation of the inflammasome. Considering that sterile particulates such as monosodium urate (MSU) crystals are capable of activating the NLRP3 inflammasome (Shi et al., 2010), we incubated MDMs with 100 μM MSU before infection with R5-tropic HIV-1_{BaL} and then analyzed their viral permissiveness. The activation of the NLRP3 inflammasome by MSU reduced the release of CAp24 capsid from human MDMs (Figure 2A) and its intracellular detection (Figure 2B) after 3 days (Figure 2A) and 6 days (Figures 2A and 2B) of infection with R5-tropic HIV-1_{BaL}. This

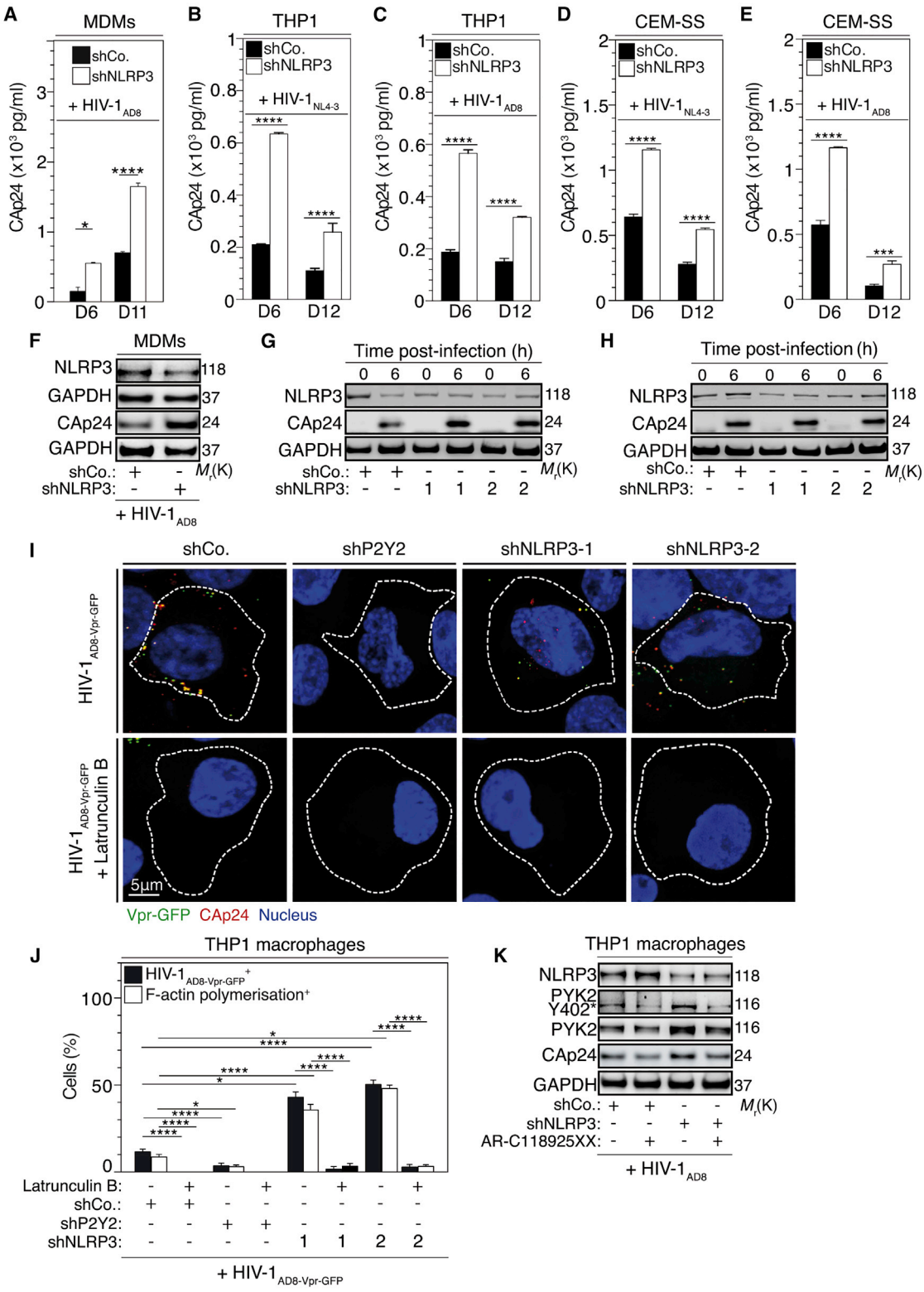

(legend on next page)

MSU-mediated inhibition of HIV-1 was more efficient than the one detected with lipopolysaccharide (LPS) (Figures 2A and 2B). To further characterize the impact of NLRP3 inflammasome activation on the early steps of HIV-1 infection, we monitored the effects of MSU treatment on intracellular HIV-1 CAp24 capsid levels (after removal of membrane bound non-internalized virus with trypsin treatment) and on the early reverse transcripts that are detected after 6 and 24 h, respectively, of infection of human MDMs with R5-tropic HIV-1_{AD8}. These data revealed that NLRP3 inflammasome activation impaired the accumulation of intracellular HIV-1 CAp24 capsid (Figure 2C) and subsequently reduced the early reverse transcripts (Figure 2E) without affecting cell viability (Figure S2A) nor the membrane expression of the viral receptors CD4 (Figure S2B) and CXCR5 (Figure S2C). Accordingly, MSU did not impair the accumulation of intracellular HIV-1 CAp24 capsid in human MDMs that were infected by the HIV-$1_{NL4\text{-}3\Delta ENV}$ variant (defective in viral envelope) pseudotyped with the vesicular stomatitis virus G protein (VSV-G) envelope, HIV-$1_{VSV\text{-}G}$ (Figure 2D). Altogether, these results demonstrate that NLRP3 inflammasome activation inhibits HIV-1 entry into host cells.

NLRP3 Protein Inhibits HIV-1 Infection by Repressing the Cytoskeletal Remodeling Required for HIV-1 Entry

We determined the role of NLRP3 inflammasome protein during the early steps of HIV-1 infection through the knockdown of NLRP3 using specific short hairpin RNA (shRNA). We observed that the depletion of NLRP3 increased the release of CAp24 capsid from human MDMs (Figure 3A and S3A), THP1 monocytes (Figures 3B, 3C, and S3B), and CEM-SS T cells (Figures 3D, 3E, and S3C) after 6, 11, or 12 days of infection with R5-tropic HIV-1_{AD8} (Figures 3A, 3C, and 3E) or X4-tropic HIV-$1_{NL4\text{-}3}$ (Figures 3B and 3D). After removing membrane-bound non-internalized HIV-1 particles by trypsinizing the cells, western blot detection of intracellular CAp24 capsid corroborated that the depletion of NLRP3 in MDMs increased cellular susceptibility to HIV-1 infection after 6 h of infection (Figure 3F). These data were confirmed by the depletion of NLRP3 in THP1 monocytes that were then infected with X4-tropic HIV-$1_{NL4\text{-}3}$ for 6 h (Figures 3G and S3D). To rule out the possibility that NLRP3 protein may also act at post-entry levels, we evaluated the effects of NLRP3 overexpression on viral yields after transfection of X4-tropic HIV-$1_{NL4\text{-}3}$ (Figure S3E) or R5-tropic HIV-1_{AD8} (Figure S3F) DNA constructs that subsequently produce infectious virions. NLRP3 overexpression (Figures S3E and S3F) did not impact the amount and infectivity of X4-tropic HIV-$1_{NL4\text{-}3}$ (Figures S3G and S3I) and R5-tropic HIV-1_{AD8} (Figures S3H and S3J) produced 48 h post transfection. Consistently, the depletion of NLRP3 failed to increase infection of target cells by HIV-$1_{VSV\text{-}G}$ (Figures 3H and S3K). These results imply that NLRP3 protein selectively inhibits receptor-mediated entry of HIV-1.

Emerging evidence has revealed important inflammasome-independent roles for ASC and CASP1 in controlling immune responses through the modulation of F-actin polymerization (Caution et al., 2015; Ippagunta et al., 2011). In our previous report (Séror et al., 2011), we demonstrated that following HIV-1 infection, P2Y2 enhances plasma membrane depolarization through the activating autophosphorylation of the proline-tyrosine kinase 2 (PYK2) on tyrosine residue 402 (PYK2Y402*) to favor the early fusion of the HIV-1 membrane and the target cell. Importantly, activated PYK2 is known to broadly modulate the F-actin rearrangement and polymerization to regulate immune cells migration, morphology or growth (Collins et al., 2010; Du et al., 2001; Okigaki et al., 2003; Ren et al., 2001; Wang et al., 2003). F-actin remodeling is also required for HIV-1 membrane fusion with target cells and entry (Jiménez-Baranda et al., 2007; Stolp and Fackler, 2011). Considering that F-actin cytoskeletal remodeling and the associated PYK2 activation both contribute to HIV-1 early viral entry (Jiménez-Baranda et al., 2007; Séror et al., 2011; Stolp and Fackler, 2011),

Figure 3. NLRP3 Inhibits HIV-1 Entry by Repressing F-Actin Polymerization

(A) HIV-1 CAp24 in cell supernatant analyzed by ELISA of control and NLRP3-depleted MDMs infected with HIV-1_{AD8} after 6 and 11 days of infection. Data are presented as means ± SEM, and significance levels are *p ≤ 0.05 and ****p ≤ 0.0001 (n = 3 independent donors), unpaired Mann-Whitney test. See also Figure S3A.

(B and C) HIV-1 CAp24 in cell supernatant analyzed by ELISA of control and NLRP3-depleted THP1 monocytes infected with X4-tropic HIV-$1_{NL4\text{-}3}$ (B) and R5-tropic HIV-1_{AD8} (C) after 6 and 12 days of infection. Data are presented as means ± SEM, and significance is ****p ≤ 0.0001 (n = 3 independent experiments), unpaired t test. See also Figure S3B.

(D and E) HIV-1 CAp24 in cell supernatant analyzed by ELISA of control and NLRP3-depleted CEM-SS T cells infected with X4-tropic HIV-$1_{NL4\text{-}3}$ (D) and R5-tropic HIV-1_{AD8} (E) after 6 and 12 days of infection. Data are presented as means ± SEM, and significance is ****p ≤ 0.0001 (n = 3 independent experiments), ANOVA test. See also Figure S3C.

(F) Intracellular CAp24 analyzed by western blot in control and NLRP3-depleted MDMs, which were infected for 6 h with R5-tropic HIV-1_{AD8}. Representative western blots of three independent donors are shown. See also Figures S3D and S3K.

(G and H) Intracellular HIV-1 CAp24 analyzed by western blot in control and NLRP3-depleted THP1 cells infected for 6 h with X4-tropic HIV-$1_{NL4\text{-}3}$ (G) or HIV-$1_{NL4\text{-}3\Delta Env}$ pseudotyped with VSV-G envelope (H). Representative western blots of three independent experiments are shown.

(I) Confocal microscopy images of HIV-1 entry (detected with CAp24 and Vpr-GFP signals) in THP1 macrophages control and depleted for P2Y2 (shP2Y2) or for NLRP3 (shNLRP3-1 and 2) and infected for 6 h with R5-tropic HIV-$1_{AD8\text{-}Vpr\text{-}GFP}$ in the presence or absence of latrunculin B (10 μM). Dashed lines indicate the cellular perimeters. The corresponding F-actin polymerization staining (with phalloidin) is shown in Figure S3L. Images are representative of three independent experiments.

(J) Cell percentage of HIV-$1_{AD8\text{-}Vpr\text{-}GFP}$ and F-actin polymerization positive cells determined by confocal microscopy as shown in (I) and in Figure S3L. Data obtained from three independent experiments are presented as means ± SEM (n = 300 cells). Significance levels are *p ≤ 0.05 and ****p ≤ 0.0001, ANOVA test.

(K) NLRP3, PYK2Y402*, PYK2, and intracellular CAp24 analyzed by western blot of control and NLRP3-depleted THP1 macrophages pretreated 18 h with AR-C118925XX (100 μM) and infected with R5-tropic HIV-1_{AD8} for 6 h treated in the presence of the drug. Western blots are representative of three independent experiments.

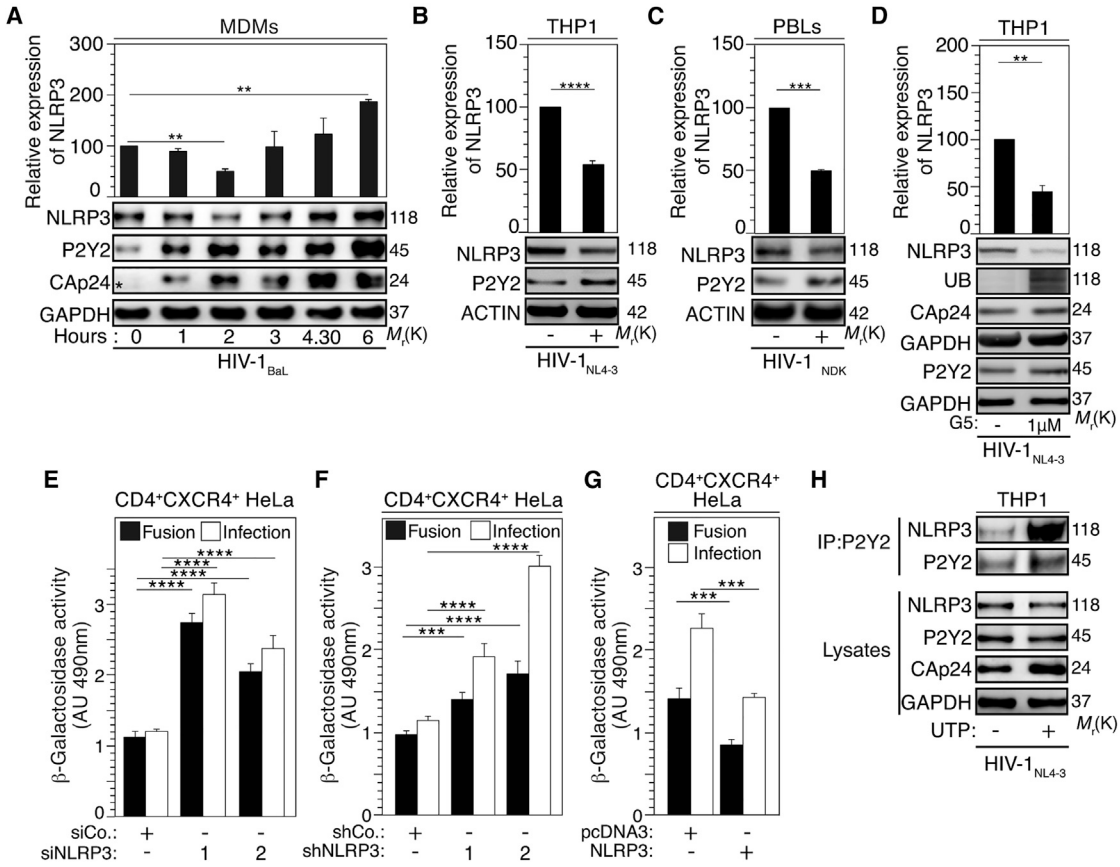

Figure 4. NLRP3 Expression Is Decreased during the Early Steps of HIV-1 Infection

(A–C) NLRP3 and P2Y2 expressions in MDMs (A), THP1 cells (B), and PHA/IL-2-stimulated human lymphocytes (C) that were infected, respectively, during indicated times (A), 6 h (B), or 3 h (C) with indicated viruses. Intracellular CAp24 level is also shown in (A). Representative western blots of three independent experiments are shown. The relative NLRP3 expression data from n = 3 independent experiments are presented as means ± SEM. Significance levels are $^{**}p \leq 0.01$, $^{***}p \leq 0.001$, and $^{****}p \leq 0.0001$, unpaired t test.

(D) THP1 cells were infected for 6 h with X4-tropic HIV-1_{NL4-3} in the presence of 1 μM G5 and analyzed by western blot for NLRP3, ubiquitinylation (UB), P2Y2, intracellular CAp24, and GAPDH expressions. Data obtained from n = 3 independent experiments are presented as means ± SEM. Significance level is $^{**}p \leq 0.01$, unpaired t test.

(E–G) Tat-inducible β-Galactosidase reporter gene expressing HeLa CD4$^+$CXCR4$^+$ cells were depleted (E and F) or transfected (G) for NLRP3 for, respectively, 48 h (E and F) or 24 h (G), co-cultured with fusogenic HIV-1 envelope (Env) expressing HeLa cells (E–G), or infected with X4-tropic HIV-1_{NL4-3} (E–G) and evaluated for HIV-1 Env-mediated fusion and for infection (E–G). Data obtained from n = 3 independent experiments are presented as means ± SEM. Significance levels are $^{***}p \leq 0.001$ and $^{****}p \leq 0.0001$, unpaired t test. See also Figures S5A, S5B, and S5C.

(H) Immunoprecipitations were performed in THP1 monocytes that were stimulated for 2 h with UTP and then infected with X4-tropic HIV-1_{NL4-3} for 6 h in the presence of UTP. Representative western blots of two independent experiments are shown. See also Figures S5L and S5M.

we hypothesized that NLRP3 may antagonize the effects of activated P2Y2 and PYK2 on F-actin remodeling upon HIV-1 infection, thereby inhibiting HIV-1 entry. Confocal microscopy analysis revealed that NLRP3 depletion increased the entry of GFP-fused viral protein (Vpr) containing viral particles (HIV-$1_{AD8\text{-}Vpr\text{-}GFP}$) (McDonald et al., 2002) into PMA-THP1 macrophages, as revealed by the intracellular detection of HIV-$1_{AD8\text{-}Vpr\text{-}GFP}$ and CAp24 (Figures 3I and 3J). The enhanced viral entry into NLRP3-depleted cells was associated with an increase of F-actin cytoskeletal polymerization (Figures 3J and S3L). Moreover, inhibition of F-actin polymerization by latrunculin B abrogated the stimulation of HIV-1 infection by NLRP3 depletion (Figures 3I, 3J, and S3L). Consistently, the selective P2Y2 antagonist AR-C118925XX abrogated the NLRP3 depletion-driven signaling pathway (as revealed by the decreased of PYK2402* and intracellular CAp24 level [Figure 3K]) in NLRP3-depleted THP1 macrophages that were infected with R5-tropic HIV-1_{AD8} for 6 h. Altogether, these results demonstrate that, independently from its contribution to the inflammasome, NLRP3 protein acts as an endogenous repressor of F-actin cytoskeletal polymerization that facilitates the P2Y2-dependent entry of HIV-1 into target cells.

NLRP3 Is Degraded during the Early Steps of HIV-1 Infection

To determine how HIV-1 may overcome the NLRP3-mediated inhibition of its entry into host cells, we simultaneously measured NLRP3 and P2Y2 expressions during infection.

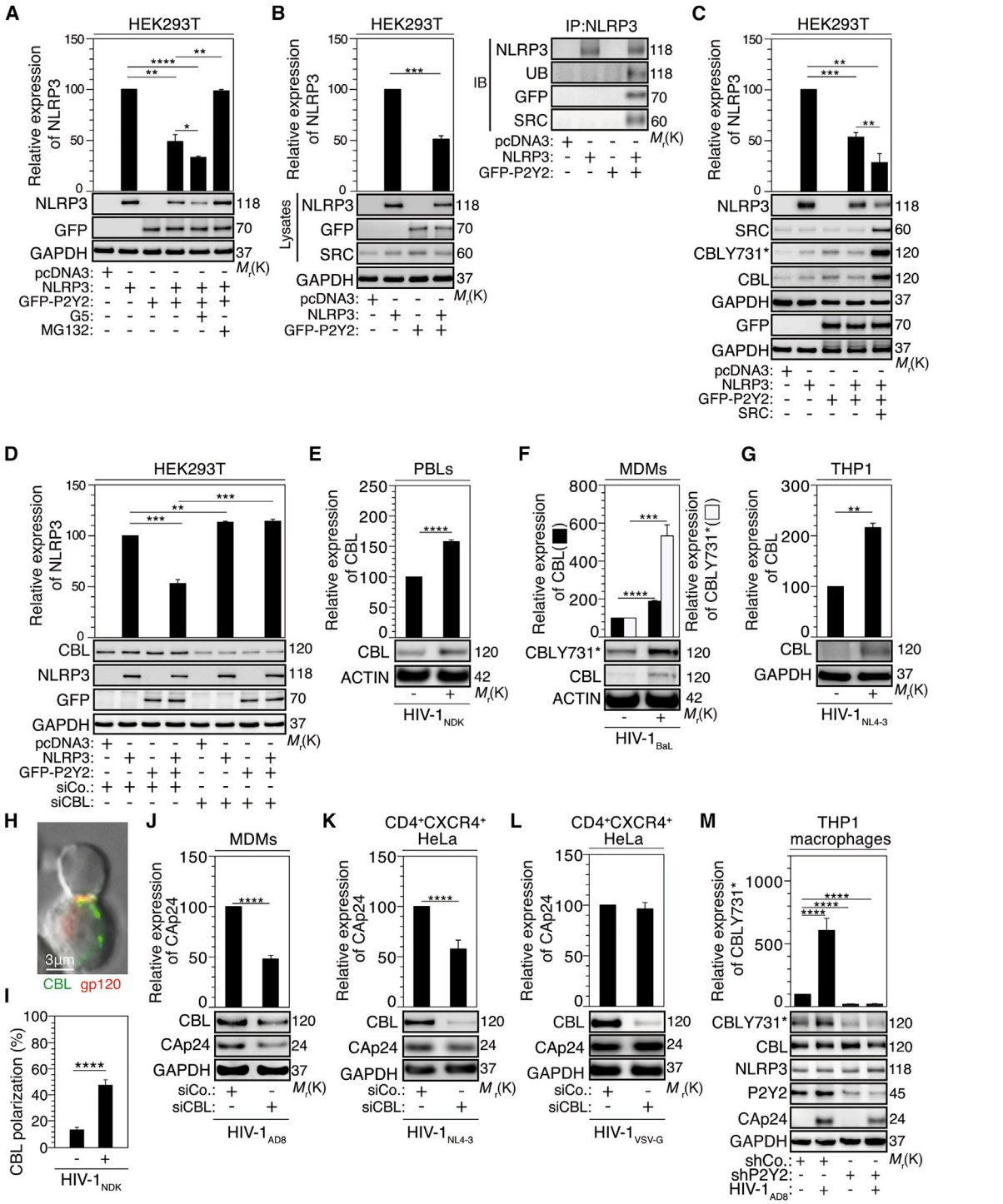

Figure 5. HIV-1 Viral Entry Is Controlled by E3 Ubiquitin Ligase CBL-Dependent Modulation of NLRP3 Expression

(A) NLRP3 and/or GFP-P2Y2 expressing cells were treated with 1 μM G5 or 10 μM MG132 and analyzed for NLRP3 and P2Y2 expressions.

(B) HEK293T cells expressing NLRP3 and GFP-P2Y2 were immunoprecipitated for NLRP3 and analyzed for ubiquitinylation (UB), SRC, NLRP3, and P2Y2 expressions.

(C) HEK293T cells expressing NLRP3, GFP-P2Y2, and/or SRC were analyzed for NLRP3, P2Y2, SRC, CBLY731*, and CBL expressions.

(D) NLRP3 and/or GFP-P2Y2 expressing cells were silenced for CBL and analyzed for NLRP3, P2Y2, and CBL expression. All protein expressions are performed using western blot. Representative western blots of three independent experiments are shown in (A)–(D). Relative expression of NLRP3 data from n = 3 independent experiments are presented as means ± SEM. Significance levels are *p ≤ 0.05, **p ≤ 0.01, ***p ≤ 0.001, and ****p ≤ 0.0001, unpaired t test.

(legend continued on next page)

Despite the fact that P2Y2 protein levels increased, NLRP3 protein levels rapidly decreased after cell-free infection of MDMs with R5-tropic HIV-1_{BaL} (Figure 4A), THP1 monocytes (Figures 4B, S4A, S4B, and S4E–S4H) and CEM-SS T cells (Figures S4C, S4D, and S4I–S4L) with X4-tropic HIV-1_{NL4-3} (Figures 4B, S4A, S4C, S4E, S4F, S4I, and S4J) or R5-tropic HIV-1_{AD8} (Figures S4B, S4D, S4G, S4H, S4K, and S4L), and PBLs with X4-tropic HIV-1_{NDK} (Figure 4C). However, NLRP3 mRNA expressions were not altered after infection of THP1 monocytes (Figures S4M and S4N) and CEM-SS T cells (Figures S4O and S4P) with X4-tropic HIV-1_{NL4-3} (Figures S4M and S4O) and R5-tropic HIV-1_{AD8} (Figures S4N and S4P). The ubiquitin isopeptidase inhibitor G5 that was previously described as an inducer of NLRP3 degradation (Py et al., 2013) decreased the protein levels of NLRP3 (Figure 4D), thus suggesting that the reduction of NLRP3 protein expression induced by HIV-1 infection must occur through post-transcriptional mechanisms. This process is associated with the enhancement of P2Y2 expression and HIV-1 permissiveness of THP1 monocytes (as indicated by the increased intracellular accumulation of HIV-1 capsid CAp24) (Figure 4D), in line with the hypothesis that NLRP3 and P2Y2 control HIV-1 entry into target cells. Consistently, we observed that the depletion or the overexpression of NLRP3 (Figures S5A–S5C) enhanced or reduced, respectively, HIV-1 Env-elicited fusion (Figures 4E–4G), the intracellular accumulation of HIV-1 CAp24 capsid (Figures S5D–S5F), and the susceptibility to HIV-1 infection (Figure 4E–4G), without affecting the expression of the HIV-1 receptor CD4 and that of its co-receptor CXCR4 (Figures S5G–S5I). Consistent with our previous report (Séror et al., 2011), we confirmed that the P2Y2 inhibitor AR-C118925XX (Figure S5J) and shRNA-mediated P2Y2 depletion (Figure S5K) impaired the entry of R5-tropic HIV-1_{AD8} into MDMs (Figure S5J) or of X4-tropic HIV-1_{NL4-3} into THP1 monocytes (Figure S5K). This effect is associated with the increased expression of NLRP3 in target cells (Figure S5K). We also evaluated the impact of the selective activation of P2Y2 by uridine triphosphate (UTP) in THP1 cells infected with X4-tropic HIV-1_{NL4-3} for 6 h on the NLRP3 and P2Y2 interaction and on the levels of NLRP3. P2Y2 activation led to a significant enhancement of the NLRP3-P2Y2 interaction associated with the degradation of NLRP3 and an increase of HIV-1 entry into cells (Figures 4H, S5L, and S5M). Altogether, these data indicate that the activation of P2Y2 occurring shortly after HIV-1 infection increases the susceptibility of cells to viral entry by inducing NLRP3 protein degradation.

HIV-1 Envelope Overcomes NLRP3 Inhibition through the Activation of the E3 Ubiquitin Ligase CBL

To define the molecular mechanisms accounting for the degradation of NLRP3 during the early steps of infection, HEK293T cells were transfected with full-length NLRP3, with GFP-tagged full-length P2Y2, or with both constructs. Co-expression of GFP-P2Y2 with NLRP3 reduced the expression of NLRP3 protein, while co-expression of NLRP3 failed to reduce the expression of GFP-P2Y2 (Figure 5A). The downregulation of NLRP3 by P2Y2 was increased by the ubiquitin isopeptidase inhibitor G5 and fully blocked by the proteasome inhibitor MG132 (Figures 5A and S6A), thus demonstrating that upon P2Y2 activation, NLRP3 is ubiquitinylated and degraded by the proteasome. Considering that the ubiquitinylation and subsequent degradation of NLRP3 can be initiated by ubiquitin ligases such as E3 ubiquitin ligase CBL through its SRC kinase-dependent phosphorylation (on tyrosine 731, CBLY731*) (Kankkunen et al., 2014; Py et al., 2013), we checked whether the kinase SRC that was previously described as a downstream target of P2Y2-dependent signaling pathway (Liu et al., 2004) may interact with NLRP3 and control its degradation through the activation of CBL. Indeed, the kinase SRC co-immunoprecipitated with NLRP3 when NLRP3 was ubiquitinylated and degraded (Figure 5B). Moreover, pharmacological inhibition of SRC with PP1 or PP2 impaired the interaction between NLRP3 and P2Y2 (Figure S6B) and favored NLRP3 accumulation in THP1 cells (Figure S6B). Moreover, in HEK293T cells, transfection of full-length SRC together with full-length NLRP3 and GFP-tagged full-length P2Y2 led to an increased expression and phosphorylation of CBL on tyrosine 731 (CBLY731*) as well as to NLRP3 degradation (Figure 5C). Since the SRC kinase is a candidate for proteasomal degradation through a CBL-dependent process (Sandilands et al., 2012), we next investigated the role of CBL in P2Y2-induced degradation of NLRP3. Indeed, CBL depletion abolished the negative effect of GFP-P2Y2 on the overall abundance of the NLRP3 protein (Figure 5D). Altogether, these results suggest that P2Y2 controls NLRP3

(E–G) PHA/IL-2-stimulated human lymphocytes (E), MDMs (F), and THP1 cells (G) were infected, respectively, for 3, 3, or 6 h with X4-tropic HIV-1_{NDK} (E), R5-tropic HIV-1_{BaL} (F), or X4-tropic HIV-1_{NL4-3} (G) and analyzed by western blot for CBLY731* and CBL relative expressions. Representative western blots of three independent experiments are shown. Relative expressions data from n = 3 independent experiments are presented as means ± SEM. Significances are **$p \leq 0.01$, ***$p \leq 0.001$, and ****$p \leq 0.0001$, unpaired t test.

(H and I) Confocal microscopy image (H) of CBL and gp120 polarization during HIV-1-infected and uninfected lymphocyte interactions. Frequencies of CBL polarization during HIV-1-infected and uninfected lymphocyte interactions are shown (I). Images are representative of three different donors. Data are presented as means ± SEM, and significance is ****$p \leq 0.0001$ (n = 3 independent donors), unpaired t test.

(J) Intracellular CAp24 analyzed by western blot and its relative expression in control and CBL-depleted MDMs were infected for 6 h with HIV-1_{AD8}. Representative western blots of three independent experiments are shown. Relative expression data from three independent experiments are presented as means ± SEM. Significance is ****$p \leq 0.0001$ (n = 3 independent donors), unpaired t test.

(K and L) Intracellular CAp24 analyzed by western blot of CBL-depleted $CD4^+CXCR4^+$ cells were infected with HIV-1_{NL4-3} (K) or HIV-1_{VSV-G} (L) for 6 h. Representative western blots of three independent experiments are shown. Relative expression from n = 3 independent experiments are presented as means ± SEM. Significance is ****$p \leq 0.0001$, unpaired t test.

(M) Expressions of CBLY731*, CBL, P2Y2, and intracellular CAp24 analyzed by western blot in control and P2Y2-depleted THP1 macrophages infected for 6 h with R5-tropic HIV-1_{AD8}. Representative western blots of three independent experiments are shown. Relative expression of CBLY731* from n = 3 independent experiments are presented as means ± SEM. Significance is ****$p \leq 0.0001$, unpaired t test.

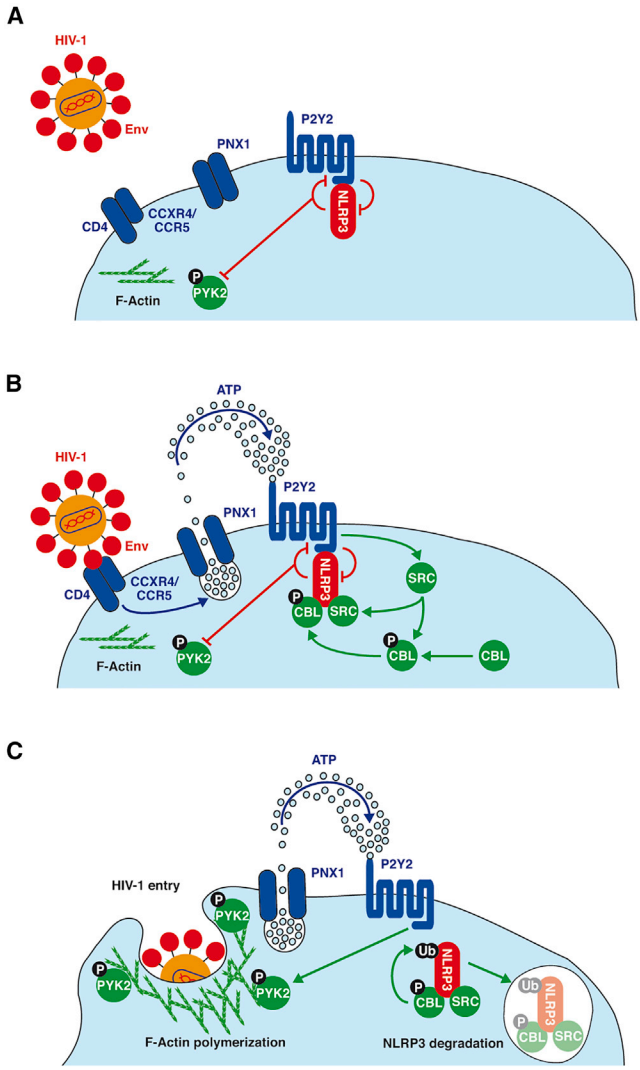

Figure 6. Model of HIV-1 Escape to NLRP3 Inhibition during the Early Steps of Viral Entry

(A–C) NLRP3 interacts constitutively with P2Y2 and suppresses the phosphorylation of PYK2 (PYK2Y402*) and F-actin polymerization in host cells (A). The binding of HIV-1 envelope to its receptor (CD4) and co-receptors (CXCR4 or CCR5) leads to rapid ATP release from host cells through pannexin-1 (PNX1) and activates P2Y2. Once activated, P2Y2 enhances its interaction with NLRP3 and activates and favors the recruitment of SRC and CBL to NLRP3 (B), leading to NLRP3 ubiquitinylation and degradation. NLRP3 degradation leads to PYK2 phosphorylation (PYK2Y402*) and subsequent F-actin polymerization, which is required for the entry of HIV-1 into host cells (C).

degradation through a pathway involving the CBL ubiquitin ligase.

Next, we studied the role of the E3 ubiquitin ligase CBL during the early steps of HIV-1 infection. We detected increased CBL expression during cell-free infection of PBLs (Figure 5E), MDMs (Figure 5F), and THP1 monocytes (Figure 5G). This process was associated with the activating phosphorylation of CBL on tyrosine 731 (CBLY731*) 3 h post-infection of macrophages with R5-tropic HIV-1_{BaL} (Figure 5F). We also studied the subcellular localization of CBL after co-culture of X4-tropic HIV-1_{NDK}-infected and uninfected PBLs. CBL polarized toward the contact sites formed between HIV-1-infected and uninfected cells (Figures 5H and 5I), where it colocalized with the HIV-1 glycoprotein gp120 (Figure 5H). Immunofluorescence microscopy confirmed that the NLRP3/P2Y2 interaction occurs at sites of viral entry during virological synapse formation between HIV-1_{NDK}-infected and uninfected lymphoblasts (Figures 1C–1E), as well as upon cell-free infection of PBLs (Figures S1I and S1J) or MDMs (Figures 1L and 1M). We finally determined whether the E3 ubiquitin ligase CBL that is involved in the regulation of NLRP3 expression (Figure 5D) and relocalizes to the HIV-1-induced virological synapse (Figures 5H and 5I) might control viral entry. MDMs (Figure 5J) or $CD4^+CXCR4^+$ HeLa cells (Figure 5K) were depleted of CBL and infected for 6 h with R5-HIV-1_{AD8} or X4-tropic HIV-1_{NL4-3}, respectively. The depletion of CBL inhibited HIV-1 entry into target cells (as indicated by reduced intracellular HIV-1 CAp24 capsid; Figures 5J and 5K). Moreover, CBL depletion failed to reduce cell permissiveness to HIV-1_{VSV-G} (Figure 5L), again suggesting that the E3 ubiquitin ligase CBL controls P2Y2-dependent viral entry mediated by the viral envelope. To demonstrate the functional link between CBL function and P2Y2 activation during HIV-1 infection, P2Y2-depleted THP1 macrophages and control cells were infected with R5-tropic HIV-1_{AD8} for 6 h. P2Y2 depletion impaired the activating phosphorylation of CBL on tyrosine 731 (CBLY731*) (Figure 5M). This effect was associated with increased expression of NLRP3 and reduced entry of HIV-1 into target cells (Figure 5M). Altogether these results suggest that the binding between HIV-1 Env and its host cell receptors (CD4 and chemokine co-receptors) induces the recruitment of the E3 ubiquitin ligase CBL to viral entry sites for modulating the functional interaction between NLRP3 and P2Y2 interaction, thus facilitating viral entry.

DISCUSSION

Deciphering the complex network of innate signaling pathways is crucial for understanding the function of immune cells (such as monocytes, macrophages, and dendritic cells) that might constitute prime targets for prophylactic or therapeutic intervention in various human pathologies (such as autoinflammatory, autoimmune, infectious, and neoplastic diseases). Innate immune signals reportedly play contrasting roles during the acute and chronic phases of HIV-1 infection (Doitsh et al., 2014). Recently, rapid inflammasome activation was reported following SIV infection of Rhesus monkeys (Barouch et al., 2016). During early SIV pathogenesis, NLRX1-mediated inhibition of inflammasome activation represses the transcription of antiviral restriction factors (such as ISG5, MX2, APOBEC3, and TRIM5) and facilitates early viral replication (Barouch et al., 2016). Here, we report that the expression of NLRP3 proteins is modulated through post-translational modifications during the early steps of HIV-1 infection and controls target cell susceptibility. We observed that following the binding of HIV-1 envelope to its host receptors (CD4, CXCR4, and/or CCR5), the interaction between NLRP3 and P2Y2 rapidly increased after HIV-1 infection, leading to the degradation of NLRP3 by

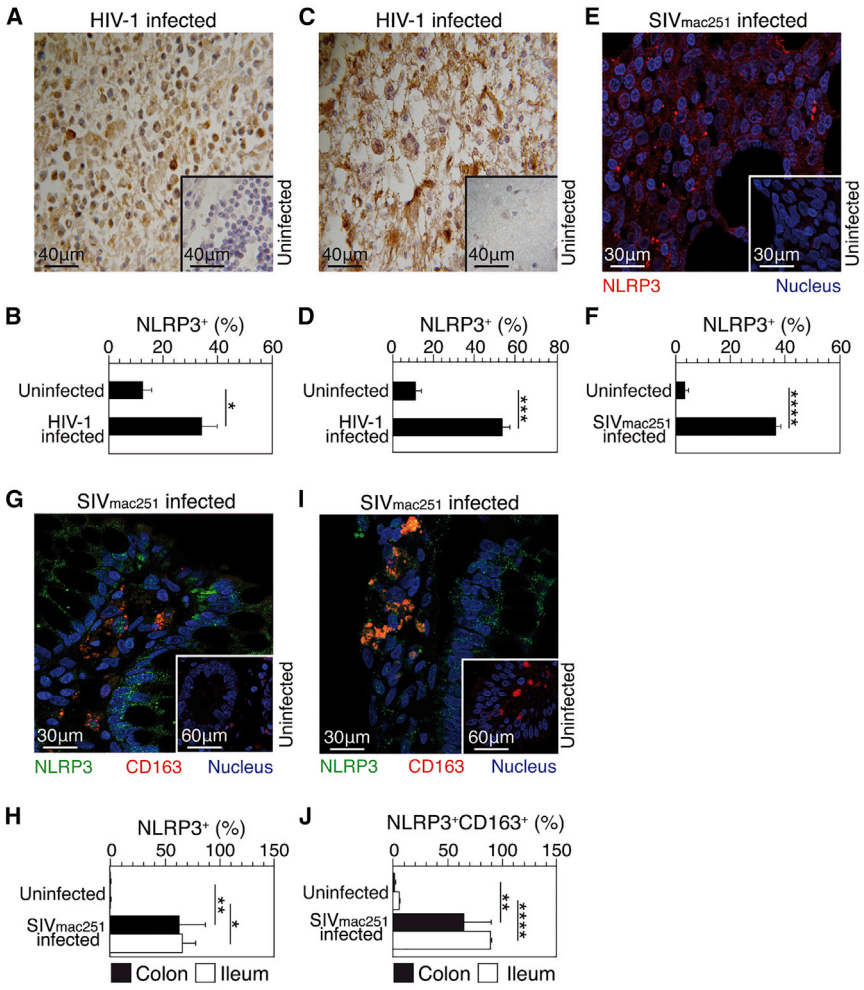

Figure 7. NLRP3 Expression Is Increased in Chronic HIV-1 and SIV Infection

(A–J) Quantification of NLRP3 and/or CD163 positive cells in lymph nodes (A, B, E, and F), brain (C and D), colon (G and H), and ileum (I and J) sections obtained from HIV-1-infected and uninfected patients (A–D) or from SIVmac251-infected and uninfected *Macaca fascicularis* (E–J) are shown. Images are representative of n = 6 HIV-1-infected and n = 4 uninfected persons in (A), of n = 3 HIV-1-infected and n = 3 uninfected persons in (C), of n = 3 SIVmac251-infected and n = 3 uninfected *Macaca fascicularis* in (G), and of n = 4 SIVmac251-infected and n = 3 uninfected *Macaca fascicularis* in (E) and (I). In (G), (H), (I), and (J), the NLRP3 expression was analyzed in CD163 positive macrophages. Data are presented in (B), (D), (F), (H), and (J) as means ± SEM. Significance levels are *$p \leq 0.05$, **$p \leq 0.01$, ***$p \leq 0.001$, and ****$p \leq 0.0001$, unpaired Mann-Whitney test.

the E3 ubiquitin ligase CBL, thus favoring P2Y2-dependent viral entry into target cells through PYK2-dependent F-actin polymerization. Indeed, the interaction between HIV-1 Env and its co-receptors enhances the interaction between NLRP3 and P2Y2 and subsequently induces the degradation of NLRP3 by CBL, favoring the activation (phosphorylation) of PYK2 (PYK2Y402*) and subsequent cytoskeletal rearrangement (through F-actin polymerization) that facilitates HIV-1 early membrane fusion with target cells (Jiménez-Baranda et al., 2007; Stolp and Fackler, 2011; Vorster et al., 2011) and hence viral entry (Figure 6).

Our results are in agreement with published works supporting the notion that polymorphisms affecting the *NLRP3* gene could influence the susceptibility to HIV-1 infection (Pontillo et al., 2010, 2012) and coinfection with *Mycobacterium tuberculosis* (Pontillo et al., 2013). Altogether, our results suggest that HIV-1 (through its envelope protein) hijacks the functional crosstalk between NLRP3 and P2Y2 to optimize its viral life cycle.

The observation that the depletion of NLRP3 enhanced the infectivity of host cells by HIV-1 suggests that NLRP3 proteins function as intrinsic inhibitory factors for HIV-1 infection. In sharp contrast to the vast majority of identified inhibitory factors that impair viral infection at post-entry steps (Harris et al., 2012), NLRP3 proteins limit HIV-1 infection by interfering with viral entry, suggesting that the NLRP3-P2Y2 interaction could be targeted for the prevention and treatment of HIV-1 infection. NLRP3 inflammasome activators (such as LPS or MSU crystals) reduce the susceptibility of HIV-1 target cells through the modulation of P2Y2-dependent F-actin remodeling. Thus, strategies designed to alter the functional interaction between NLRP3 and P2Y2 could effectively block HIV-1 infection. Nevertheless, the identification of the inflammasome inhibitor NLRX1 as transcriptional repressor of restriction factors that impair viral replication (Barouch et al., 2016) underlines the complexity of signaling pathways elicited by NLRP3 family members during the early steps of HIV-1 infection. Further molecular investigations are required to fully understand the role of NLRP3 family members during these viral steps. Future investigations must address the impact of the functional NLRP3-P2Y2 interaction on cellular regulators that are known to affect cortical F-actin rearrangement and to HIV-1 infection such as LIM domain kinase 1 (Vorster et al., 2011), moesin (Barrero-Villar et al., 2009), filamin-A (Jiménez-Baranda et al., 2007), and cofilin (Yoder et al., 2008).

There may be differences between the acute and the prolonged effects of HIV-1 on the aforementioned regulatory system. Indeed, immunoreactive NLRP3 was detected at higher levels in lymph nodes (Figures 7A and 7B) and in the frontal cortex (Figures 7C and 7D) from untreated HIV-1 carriers, as compared with uninfected specimens. Similar results were obtained when comparing control tissues from the non-human primate *Macaca fascicularis* with lymph nodes (Figures 7E and 7F) or intestinal tissues (colon in Figures 7G and 7H; ileum in Figures 7I and 7J) from macaques infected with SIV_{mac251}.

NLRP3 expression was preferentially observed in CD163$^+$ macrophages (Figures 7G, 7I, and 7J) that are known to express P2Y2 (Elliott et al., 2009). After 21 days of infection of THP1 monocytes and CEM-SS T cells with X4- and R5-tropic viruses, respectively, NLRP3 protein expression was increased (Figures S7A–S7F, S7I, and S7J), although no modification of NLRP3 mRNA levels was detectable (Figures S7M–S7P). P2Y2 protein expression did not change in CEM-SS T cells but increased after 21 days of infection of THP1 monocytes (Figures S7G, S7H, S7K, and S7L). Altogether, these results suggest that the molecular mechanisms involved in the enhanced interaction between NLRP3 and P2Y2 that is detected during chronic infection with HIV-1 may be distinct from those detected in the early steps of HIV-1 infection. The increased NLRP3 expression during chronic HIV-1 infection is consistent with recent findings showing that HIV-1 activates NLRP3 inflammasome through Tat and Vpr proteins in lymphocytes, microglial cells, and macrophages (Bandera et al., 2018; Chivero et al., 2017; Haque et al., 2016; Mamik et al., 2017). Thus, NLRP3 may play a dual opposite role during early steps of infection by inhibiting viral entry and at the later post-entry steps by contributing to neuroinflammation and immune activation associated with HIV-1 infection.

The blockade of immune checkpoints in lymphocytes has recently emerged as a new and promising approach for treating both chronic viral infection and cancer. Here, we identified a functional interaction that acts on myeloid cells and that could be exploited for the development of HIV vaccines or therapeutic combinations to cure HIV infection (Barouch et al., 2016) and potentially other viral infections (such as hepatitis B and C). In addition, it appears likely that the NLRP3-P2Y2 interaction could be manipulated for the treatment of HIV-1-associated brain disease, which is also associated with strong activation of the NLRP3 inflammasome (Walsh et al., 2014). Future studies should explore the possibility of modulating the NLRP3-P2Y2 functional interaction with the aim of treating human diseases that are triggered by excessive activation of the NLRP3 inflammasome, such as cryopyrin-associated periodic syndromes (Agostini et al., 2004), rheumatoid arthritis (Vande Walle et al., 2014), obesity (Vandanmagsar et al., 2011), or Alzheimer's disease (Halle et al., 2008).

Thus, our data demonstrate a constitutive interaction between NLRP3 and P2Y2 that could be targeted to reduce viral propagation and improve the immune response against HIV infection.

STAR★METHODS

Detailed methods are provided in the online version of this paper and include the following:

- KEY RESOURCES TABLE
- LEAD CONTACT AND MATERIALS AVAILABILITY
- EXPERIMENTAL MODEL AND SUBJECT DETAILS
  - Cell lines
  - Primary Cells
  - Non-Human primates
  - Human autopsies
- METHODS DETAILS
  - Plasmids and transfections
  - siRNA- and shRNA-mediated knockdowns
  - Virus productions
  - Viral infections
  - Immunofluorescence
  - Western blots and immunoprecipitations
  - Flow cytometry
  - Quantitative PCR (qPCR)
- QUANTIFICATION AND STATISTICAL ANALYSIS
- DATA AND CODE AVAILABILITY

SUPPLEMENTAL INFORMATION

Supplemental Information can be found online at https://doi.org/10.1016/j.celrep.2019.02.095.

ACKNOWLEDGMENTS

This work was supported by funds from Agence Nationale de la Recherche (ANR-10-IBHU-0001, ANR-10-LABX33, and ANR-11-IDEX-003-01), Electricité de France, Fondation Gustave Roussy, Institut National du Cancer (INCA 9414), NATIXIS, Sidaction, and the French National Agency for Research on AIDS and Viral Hepatitis (ANRSH) (to J.-L.P.); Ligue contre le Cancer (équipe labellisée), Agence National de la Recherche (ANR) – Projets blancs, Cancéropôle Ile-de-France, Institut National du Cancer (INCa), Institut Universitaire de France, the LabEx Immuno-Oncology, the RHU Torino Lumière, the SIRIC Stratified Oncology Cell DNA Repair and Tumor Immune Elimination (SOCRATE), and the SIRIC Cancer Research and Personalized Medicine (CARPEM) (to G.K.); MIUR (PRIN 2012 and FIRB), the Ministry of Health of Italy "Ricerca Corrente" and "Ricerca Finalizzata," AIRC and European Commission "Transpath" Marie Curie Project (to M.P.); and Electricité de France and Fondation Gustave Roussy (to E.D.). A.P. and A.A. are recipients of PhD fellowships and a post-doc fellowship, respectively, from Agence Nationale de Recherche sur le Sida et sur les Hépatites (ANRSH). S.Q.R. is supported by Higher Education Commission (Pakistan) and by the Laboratory of Excellence LERMIT with a grant from ANR (ANR-10-LABX-33) under the program "Investissements d'Avenir" ANR-11-IDEX-0003-01. M.C. is funded by a postdoctoral fellowship from Sidaction. We gratefully acknowledge Y. Lecluse and S. Salome-Desnoulez for technical support.

AUTHOR CONTRIBUTIONS

Conceptualization, J.-L.P.; Methodology, J.-L.P., A.P., and A.A.; Investigation, A.P., A.A., M.C., H.S., F.S., R.N., Q.W., Z.M., L.V., S.Q.R., F.L., M.T., H.D., B.P.-B., and N.D.-B.; Validation, J.-L.P.; Formal Analysis, A.P. and A.A.; Writing – Original Draft, J.-L.P., A.P., and A.A.; Writing – Review & Editing, J.-L.P., A.A., G.K., and D.M.O.; Resources, O.D., R.L.G., O.L., A.S.-C., G.P., E.S., E.D., M.P., M.-L.G., and G.K.; Supervision, J.-L.P.

DECLARATION OF INTERESTS

The authors declare no competing interests.

Received: June 27, 2018
Revised: January 8, 2019
Accepted: February 22, 2019
Published: September 24, 2019

REFERENCES

Agostini, L., Martinon, F., Burns, K., McDermott, M.F., Hawkins, P.N., and Tschopp, J. (2004). NALP3 forms an IL-1beta-processing inflammasome with increased activity in Muckle-Wells autoinflammatory disorder. Immunity *20*, 319–325.

Allouch, A., Di Primio, C., Alpi, E., Lusic, M., Arosio, D., Giacca, M., and Cereseto, A. (2011). The TRIM family protein KAP1 inhibits HIV-1 integration. Cell Host Microbe *9*, 484–495.

Allouch, A., David, A., Amie, S.M., Lahouassa, H., Chartier, L., Margottin-Goguet, F., Barré-Sinoussi, F., Kim, B., Sáez-Cirión, A., and Pancino, G. (2013). p21-mediated RNR2 repression restricts HIV-1 replication in macrophages by inhibiting dNTP biosynthesis pathway. Proc. Natl. Acad. Sci. USA *110*, E3997–E4006.

Bandera, A., Masetti, M., Fabbiani, M., Biasin, M., Muscatello, A., Squillace, N., Clerici, M., Gori, A., and Trabattoni, D. (2018). The NLRP3 Inflammasome Is Upregulated in HIV-Infected Antiretroviral Therapy-Treated Individuals with Defective Immune Recovery. Front. Immunol. *9*, 214.

Barouch, D.H., Ghneim, K., Bosche, W.J., Li, Y., Berkemeier, B., Hull, M., Bhattacharyya, S., Cameron, M., Liu, J., Smith, K., et al. (2016). Rapid Inflammasome Activation following Mucosal SIV Infection of Rhesus Monkeys. Cell *165*, 656–667.

Barrero-Villar, M., Cabrero, J.R., Gordón-Alonso, M., Barroso-González, J., Alvarez-Losada, S., Muñoz-Fernández, M.A., Sánchez-Madrid, F., and Valenzuela-Fernández, A. (2009). Moesin is required for HIV-1-induced CD4-CXCR4 interaction, F-actin redistribution, membrane fusion and viral infection in lymphocytes. J. Cell Sci. *122*, 103–113.

Caillet, M., Janvier, K., Pelchen-Matthews, A., Delcroix-Genête, D., Camus, G., Marsh, M., and Berlioz-Torrent, C. (2011). Rab7A is required for efficient production of infectious HIV-1. PLoS Pathog. *7*, e1002347.

Caution, K., Gavrilin, M.A., Tazi, M., Kanneganti, A., Layman, D., Hoque, S., Krause, K., and Amer, A.O. (2015). Caspase-11 and caspase-1 differentially modulate actin polymerization via RhoA and Slingshot proteins to promote bacterial clearance. Sci. Rep. *5*, 18479.

Chen, I.Y., and Ichinohe, T. (2015). Response of host inflammasomes to viral infection. Trends Microbiol. *23*, 55–63.

Chivero, E.T., Guo, M.L., Periyasamy, P., Liao, K., Callen, S.E., and Buch, S. (2017). HIV-1 Tat Primes and Activates Microglial NLRP3 Inflammasome-Mediated Neuroinflammation. J. Neurosci. *37*, 3599–3609.

Collins, M., Bartelt, R.R., and Houtman, J.C. (2010). T cell receptor activation leads to two distinct phases of Pyk2 activation and actin cytoskeletal rearrangement in human T cells. Mol. Immunol. *47*, 1665–1674.

David, A., Sáez-Cirión, A., Versmisse, P., Malbec, O., Iannascoli, B., Herschke, F., Lucas, M., Barré-Sinoussi, F., Mouscadet, J.F., Daëron, M., and Pancino, G. (2006). The engagement of activating FcgammaRs inhibits primate lentivirus replication in human macrophages. J. Immunol. *177*, 6291–6300.

Delelis, O., Malet, I., Na, L., Tchertanov, L., Calvez, V., Marcelin, A.G., Subra, F., Deprez, E., and Mouscadet, J.F. (2009). The G140S mutation in HIV integrases from raltegravir-resistant patients rescues catalytic defect due to the resistance Q148H mutation. Nucleic Acids Res. *37*, 1193–1201.

Dioszeghy, V., Benlhassan-Chahour, K., Delache, B., Dereuddre-Bosquet, N., Aubenque, C., Gras, G., Le Grand, R., and Vaslin, B. (2006). Changes in soluble factor-mediated CD8+ cell-derived antiviral activity in cynomolgus macaques infected with simian immunodeficiency virus SIVmac251: relationship to biological markers of progression. J. Virol. *80*, 236–245.

Doitsh, G., Cavrois, M., Lassen, K.G., Zepeda, O., Yang, Z., Santiago, M.L., Hebbeler, A.M., and Greene, W.C. (2010). Abortive HIV infection mediates CD4 T cell depletion and inflammation in human lymphoid tissue. Cell *143*, 789–801.

Doitsh, G., Galloway, N.L., Geng, X., Yang, Z., Monroe, K.M., Zepeda, O., Hunt, P.W., Hatano, H., Sowinski, S., Muñoz-Arias, I., and Greene, W.C. (2014). Cell death by pyroptosis drives CD4 T-cell depletion in HIV-1 infection. Nature *505*, 509–514.

Du, Q.S., Ren, X.R., Xie, Y., Wang, Q., Mei, L., and Xiong, W.C. (2001). Inhibition of PYK2-induced actin cytoskeleton reorganization, PYK2 autophosphorylation and focal adhesion targeting by FAK. J. Cell Sci. *114*, 2977–2987.

Elliott, M.R., Chekeni, F.B., Trampont, P.C., Lazarowski, E.R., Kadl, A., Walk, S.F., Park, D., Woodson, R.I., Ostankovich, M., Sharma, P., et al. (2009). Nucleotides released by apoptotic cells act as a find-me signal to promote phagocytic clearance. Nature *461*, 282–286.

Halle, A., Hornung, V., Petzold, G.C., Stewart, C.R., Monks, B.G., Reinheckel, T., Fitzgerald, K.A., Latz, E., Moore, K.J., and Golenbock, D.T. (2008). The NALP3 inflammasome is involved in the innate immune response to amyloid-beta. Nat. Immunol. *9*, 857–865.

Haque, S., Lan, X., Wen, H., Lederman, R., Chawla, A., Attia, M., Bongu, R.P., Husain, M., Mikulak, J., Saleem, M.A., et al. (2016). HIV Promotes NLRP3 Inflammasome Complex Activation in Murine HIV-Associated Nephropathy. Am. J. Pathol. *186*, 347–358.

Harris, R.S., Hultquist, J.F., and Evans, D.T. (2012). The restriction factors of human immunodeficiency virus. J. Biol. Chem. *287*, 40875–40883.

Hazleton, J.E., Berman, J.W., and Eugenin, E.A. (2012). Purinergic receptors are required for HIV-1 infection of primary human macrophages. J. Immunol. *188*, 4488–4495.

He, Y., Varadarajan, S., Muñoz-Planillo, R., Burberry, A., Nakamura, Y., and Núñez, G. (2014). 3,4-methylenedioxy-β-nitrostyrene inhibits NLRP3 inflammasome activation by blocking assembly of the inflammasome. J. Biol. Chem. *289*, 1142–1150.

Ippagunta, S.K., Malireddi, R.K., Shaw, P.J., Neale, G.A., Vande Walle, L., Green, D.R., Fukui, Y., Lamkanfi, M., and Kanneganti, T.D. (2011). The inflammasome adaptor ASC regulates the function of adaptive immune cells by controlling Dock2-mediated Rac activation and actin polymerization. Nat. Immunol. *12*, 1010–1016.

Jiménez-Baranda, S., Gómez-Moutón, C., Rojas, A., Martínez-Prats, L., Mira, E., Ana Lacalle, R., Valencia, A., Dimitrov, D.S., Viola, A., Delgado, R., et al. (2007). Filamin-A regulates actin-dependent clustering of HIV receptors. Nat. Cell Biol. *9*, 838–846.

Kankkunen, P., Välimäki, E., Rintahaka, J., Palomäki, J., Nyman, T., Alenius, H., Wolff, H., and Matikainen, S. (2014). Trichothecene mycotoxins activate NLRP3 inflammasome through a P2X7 receptor and Src tyrosine kinase dependent pathway. Hum. Immunol. *75*, 134–140.

Liu, J., Liao, Z., Camden, J., Griffin, K.D., Garrad, R.C., Santiago-Pérez, L.I., González, F.A., Seye, C.I., Weisman, G.A., and Erb, L. (2004). Src homology 3 binding sites in the P2Y2 nucleotide receptor interact with Src and regulate activities of Src, proline-rich tyrosine kinase 2, and growth factor receptors. J. Biol. Chem. *279*, 8212–8218.

Mamik, M.K., Hui, E., Branton, W.G., McKenzie, B.A., Chisholm, J., Cohen, E.A., and Power, C. (2017). HIV-1 Viral Protein R Activates NLRP3 Inflammasome in Microglia: implications for HIV-1 Associated Neuroinflammation. J. Neuroimmune Pharmacol. *12*, 233–248.

McDonald, D., Vodicka, M.A., Lucero, G., Svitkina, T.M., Borisy, G.G., Emerman, M., and Hope, T.J. (2002). Visualization of the intracellular behavior of HIV in living cells. J. Cell Biol. *159*, 441–452.

Monroe, K.M., Yang, Z., Johnson, J.R., Geng, X., Doitsh, G., Krogan, N.J., and Greene, W.C. (2014). IFI16 DNA sensor is required for death of lymphoid CD4 T cells abortively infected with HIV. Science *343*, 428–432.

Okigaki, M., Davis, C., Falasca, M., Harroch, S., Felsenfeld, D.P., Sheetz, M.P., and Schlessinger, J. (2003). Pyk2 regulates multiple signaling events crucial for macrophage morphology and migration. Proc. Natl. Acad. Sci. USA *100*, 10740–10745.

Perfettini, J.L., Roumier, T., Castedo, M., Larochette, N., Boya, P., Raynal, B., Lazar, V., Ciccosanti, F., Nardacci, R., Penninger, J., et al. (2004). NF-kappaB and p53 are the dominant apoptosis-inducing transcription factors elicited by the HIV-1 envelope. J. Exp. Med. *199*, 629–640.

Perfettini, J.L., Castedo, M., Nardacci, R., Ciccosanti, F., Boya, P., Roumier, T., Larochette, N., Piacentini, M., and Kroemer, G. (2005). Essential role of p53 phosphorylation by p38 MAPK in apoptosis induction by the HIV-1 envelope. J. Exp. Med. *201*, 279–289.

Pontillo, A., Brandão, L.A., Guimarães, R.L., Segat, L., Athanasakis, E., and Crovella, S. (2010). A 3'UTR SNP in NLRP3 gene is associated with susceptibility to HIV-1 infection. J. Acquir. Immune Defic. Syndr. *54*, 236–240.

Pontillo, A., Oshiro, T.M., Girardelli, M., Kamada, A.J., Crovella, S., and Duarte, A.J. (2012). Polymorphisms in inflammasome' genes and susceptibility to HIV-1 infection. J. Acquir. Immune Defic. Syndr. *59*, 121–125.

Pontillo, A., Carvalho, M.S., Kamada, A.J., Moura, R., Schindler, H.C., Duarte, A.J., and Crovella, S. (2013). Susceptibility to Mycobacterium tuberculosis infection in HIV-positive patients is associated with CARD8 genetic variant. J. Acquir. Immune Defic. Syndr. *63*, 147–151.

Py, B.F., Kim, M.S., Vakifahmetoglu-Norberg, H., and Yuan, J. (2013). Deubiquitination of NLRP3 by BRCC3 critically regulates inflammasome activity. Mol. Cell *49*, 331–338.

Ren, X.R., Du, Q.S., Huang, Y.Z., Ao, S.Z., Mei, L., and Xiong, W.C. (2001). Regulation of CDC42 GTPase by proline-rich tyrosine kinase 2 interacting with PSGAP, a novel pleckstrin homology and Src homology 3 domain containing rhoGAP protein. J. Cell Biol. *152*, 971–984.

Saïdi, H., Melki, M.T., and Gougeon, M.L. (2008). HMGB1-dependent triggering of HIV-1 replication and persistence in dendritic cells as a consequence of NK-DC cross-talk. PLoS ONE *3*, e3601.

Sandilands, E., Serrels, B., Wilkinson, S., and Frame, M.C. (2012). Src-dependent autophagic degradation of Ret in FAK-signalling-defective cancer cells. EMBO Rep. *13*, 733–740.

Séror, C., Melki, M.T., Subra, F., Raza, S.Q., Bras, M., Saïdi, H., Nardacci, R., Voisin, L., Paoletti, A., Law, F., et al. (2011). Extracellular ATP acts on P2Y2 purinergic receptors to facilitate HIV-1 infection. J. Exp. Med. *208*, 1823–1834.

Seye, C.I., Yu, N., González, F.A., Erb, L., and Weisman, G.A. (2004). The P2Y2 nucleotide receptor mediates vascular cell adhesion molecule-1 expression through interaction with VEGF receptor-2 (KDR/Flk-1). J. Biol. Chem. *279*, 35679–35686.

Shi, Y., Mucsi, A.D., and Ng, G. (2010). Monosodium urate crystals in inflammation and immunity. Immunol. Rev. *233*, 203–217.

Stolp, B., and Fackler, O.T. (2011). How HIV takes advantage of the cytoskeleton in entry and replication. Viruses *3*, 293–311.

Swartz, T.H., Esposito, A.M., Durham, N.D., Hartmann, B.M., and Chen, B.K. (2014). P2X-selective purinergic antagonists are strong inhibitors of HIV-1 fusion during both cell-to-cell and cell-free infection. J. Virol. *88*, 11504–11515.

Towers, G.J., and Noursadeghi, M. (2014). Interactions between HIV-1 and the cell-autonomous innate immune system. Cell Host Microbe *16*, 10–18.

Vandanmagsar, B., Youm, Y.H., Ravussin, A., Galgani, J.E., Stadler, K., Mynatt, R.L., Ravussin, E., Stephens, J.M., and Dixit, V.D. (2011). The NLRP3 inflammasome instigates obesity-induced inflammation and insulin resistance. Nat. Med. *17*, 179–188.

Vande Walle, L., Van Opdenbosch, N., Jacques, P., Fossoul, A., Verheugen, E., Vogel, P., Beyaert, R., Elewaut, D., Kanneganti, T.D., van Loo, G., and Lamkanfi, M. (2014). Negative regulation of the NLRP3 inflammasome by A20 protects against arthritis. Nature *512*, 69–73.

Vorster, P.J., Guo, J., Yoder, A., Wang, W., Zheng, Y., Xu, X., Yu, D., Spear, M., and Wu, Y. (2011). LIM kinase 1 modulates cortical actin and CXCR4 cycling and is activated by HIV-1 to initiate viral infection. J. Biol. Chem. *286*, 12554–12564.

Walsh, J.G., Reinke, S.N., Mamik, M.K., McKenzie, B.A., Maingat, F., Branton, W.G., Broadhurst, D.I., and Power, C. (2014). Rapid inflammasome activation in microglia contributes to brain disease in HIV/AIDS. Retrovirology *11*, 35.

Wang, Q., Xie, Y., Du, Q.S., Wu, X.J., Feng, X., Mei, L., McDonald, J.M., and Xiong, W.C. (2003). Regulation of the formation of osteoclastic actin rings by proline-rich tyrosine kinase 2 interacting with gelsolin. J. Cell Biol. *160*, 565–575.

Yoder, A., Yu, D., Dong, L., Iyer, S.R., Xu, X., Kelly, J., Liu, J., Wang, W., Vorster, P.J., Agulto, L., et al. (2008). HIV envelope-CXCR4 signaling activates cofilin to overcome cortical actin restriction in resting CD4 T cells. Cell *134*, 782–792.

STAR★METHODS

KEY RESOURCES TABLE

REAGENT or RESOURCE	SOURCE	IDENTIFIER
Antibodies		
CD71 (PE)	BD Pharmingen	555537; RRID: AB_395921
CD184 (CXCR4) (PE-Cy^{tm}5)	BD Pharmingen	555975; RRID: AB_396268
CD206 (FITC)	BD Pharmingen	551135; RRID: AB_394065
CD206 (Alexa Fluor 647)	ABD Serotec	MCA2235A647; RRID: AB_324890
CD4 (FITC)	BD Pharmingen	555346; RRID: AB_395751
CD163 (Alexa Fuor 647)	BD Pharmingen	562669; RRID: AB_2737710
CD163	BD Pharmingen	556017; RRID: AB_396295
CD11b (APC-Cy7)	BD Pharmingen	557657; RRID: AB_396772
CD163 (FITC)	BioLegend	333617; RRID: AB_2563093
CD14 (PE)	ebioscience	12-0149-42; RRID: AB_10598367
Mouse and Rabbit TrueBlot® ULTRA	ebioscience	18-8817 and 18-8816; RRID: AB_2610849 and AB_2610847
HIV-1 p24 (clone KC57)(FITC)	Beckman Coulter	CO6604665; RRID: AB_1575987
c-CBL (clone D4E10)	Cell Signaling	#8447; RRID: AB_10860763
Phospho-c-CBL Tyr731 (c-CBLY731*)	Cell Signaling	#3554; RRID: AB_2070452
GFP XP® (clone D5.1)	Cell Signaling	#2956; RRID: AB_1196615
PYK2 (clone 5E2)	Cell Signaling	#3480; RRID: AB_2174093
Pospho-PYK2 (Tyr402) (PYK2Y402*)	Cell Signaling	#3291; RRID: AB_2300530
SRC (clone 36D10)	Cell Signaling	#2109; RRID: AB_2106059
Phospho-SRC (Tyr416) (SRCY416*)	Cell Signaling	#2101; RRID: AB_331697
Beta-Actin (HRP)	Abcam	ab49900; RRID: AB_867494
NLRP3 (Cryo-2)	Adipogen	AG-20B-0014-C100; RRID: AB_2490202
NLRP3	Sigma-Aldrich	HPA017374; RRID: AB_1846750
P2Y2	Alomone	#APR-010; RRID: AB_2040078
Ubiquitin (clone P4D1)	Santa Cruz	sc-8017; RRID: AB_628423
FLAG ™	Sigma-Aldrich	F7425; RRID: AB_439687
GAPDH	Millipore	MAB374; RRID: AB_2107445
CAp24 (42-50)	NIH AIDS Reagent Program	4250
CAp24	Abcam	ab9044; RRID: AB_306962
gp120 (2G12)	NIH AIDS Reagent Program	1476
Bacterial and Virus Strains		
HIV-1_{NL4-3}	J.-L. Perfettini	(Séror et al., 2011)
HIV-$1_{NL4-3\Delta ENV}$	J.-L. Perfettini	(Séror et al., 2011)
HIV-1_{AD8}	NIH AIDS Reagent program	11346
HIV-1_{NDK}	M-L. Gougeon	(Saïdi et al., 2008)
HIV-1_{BaL}	NIH AIDS Reagent program	510
Biological Samples		
Human brain and lymph nodes tissues	National Institute for Infectious diseases Lazzaro Spallanzani http://www.inmi.it/index.htm	N/A
Macaca fascicularis lymph nodes, colon and ileum tissues	CEA, DSV/iMETI, Division of Immunology-Virology, IDMIT, France http://jacob.cea.fr/drf/ifrancoisjacob/Pages/Departements/IDMIT/laboratoires.aspx	N/A

(*Continued on next page*)

Continued

REAGENT or RESOURCE	SOURCE	IDENTIFIER
Human Blood Buffy coats	French blood bank (Etablissement Français du sang (EFS)) https://dondesang.efs.sante.fr/	B31111
Chemicals, Peptides, and Recombinant Proteins		
Alexa Fluor 594 phalloidin	Invitrogen	A12381
Recombinant Human and mouse M-CSF	PeproTech	300-25, 315-02
Recombinant human IL-2	PeproTech	200-02
PHA	Sigma	L8754
X-Gal	Sigma-Aldrich	B4252
Z-Leu-Leu-Leu-al (MG132)	Sigma-Aldrich	C2211
Anti-FLAG®M2 Affinity Gel	Sigma-Aldrich	A2220
Benzonase	Novagen®	71206-3
AR-C118925XX	Tocris	4890
Latrunculin B	Sigma-Aldrich	L5288
Oligofectamine	Invitrogen	58303
Puromycin	Invivogen	ant-pr-1
PMA	Invivogen	tlrl-pma
MSU	Invivogen	tlrl-msu
INTERFERin	Polyplus Transfection	409-10
UTP	Sigma	U6875
PP1	Sigma-Aldrich	P0040
PP2	Sigma-Aldrich	P0042
G5	Calbiochem	#662125
Fugene	Promega	E2312
PHA	Sigma	L8754
Critical Commercial Assays		
ELISA p24	Perkin Elmer	NEK050A
eta-galactosidase assay kit	Roche	10745731001
LDH assay kit	Roche	04744926001
Taqman universal Master Mix II, no UNG	ThermoFisher Scientific	4440040
Deposited data		
Western blot source data	This paper	Mendeley data https://doi.org/10.17632/6bxgc4h4m2.1
Experimental Models: Cell Lines		
HeLa $CD4^+$-$CXCR4^+$	J.-L. Perfettini	(Séror et al., 2011)
HeLa Env^+	J.-L. Perfettini	(Séror et al., 2011)
TZM-bl	NIH AIDS Reagent Program	8129
HEK293T	M. Caillet	(Caillet et al., 2011)
CEM-SS	A. Allouch	(Allouch et al., 2011)
THP1	ATCC	ATCC TIB202
THP1 PLKO empty control	This paper	N/A
THP1 PLKO shNLRP3.1	This paper	N/A
THP1 PLKO shNLRP3.2	This paper	N/A
THP1 PLKO shP2Y2	This paper	N/A
Human Blood Buffy coats	French blood bank (Etablissement Français du sang (EFS)) https://dondesang.efs.sante.fr/	B31111
Experimental Models: Organisms/Strains		
Macaca fascicularis	CEA, DSV/iMETI, Division of Immunology-Virology, IDMIT, France http://jacob.cea.fr/drf/ifrancoisjacob/Pages/Departements/IDMIT/laboratoires.aspx	N/A

(*Continued on next page*)

Continued

REAGENT or RESOURCE	SOURCE	IDENTIFIER
Oligonucleotides		
NLRP3 Taqman predesigned probe	ThermoFisher scientific	4331182 (Hs00918082_m1)
GAPDH TaqMan predesigned probe	ThermoFisher scientific	4331182 (Hs02758991_g1)
siRNA control for siNLRP3 1 and 2	This paper (Table S1)	N/A
siNLRP3 1 and 2 siRNAs	This paper (Table S1)	N/A
siGenome Non Targeting SMART siRNA Pool for SMART pool siRNA	Dharmacon (Table S1)	D-001206-13-20
siGENOME SMART pool human CBL siRNA	Dharmacon (Table S1)	M-003003-02-0005
Early Reverse transcripts primers and probes	G. Pancino (Table S1)	(David et al., 2006)
PLKO.1- shRNAs	This paper (Table S1)	N/A
Recombinant DNA		
pUNO-NLRP3	InvivoGen	puno1-hnalp3
pFlag-Luciferase	A. Allouch	(Allouch et al., 2011)
3×Flag-pcDNA3	G. Nunez	(He et al., 2014)
3×Flag-pcDNA3 NLRP3	G. Nunez	(He et al., 2014)
pEFGP-N1-P2Y2	L. Erb	(Seye et al., 2004)
pGFP-Vpr	G. Pancino	NA
pHIV-1_{NL4-3}	J.-L. Perfettini	(Séror et al., 2011)
pHIV-$1_{NL4-3\Delta ENV}$	J.-L. Perfettini	(Séror et al., 2011)
pHIV-1_{AD8}	NIH AIDS Reagent program	(Séror et al., 2011)
pMDG-VSV-G	J.-L. Perfettini	(Séror et al., 2011)
pCMV GAG-POL-HIV	M. Caillet	(Caillet et al., 2011)
Software and Algorithms		
Image J	https://imagej.nih.gov/ij/	N/A
Icy	http://icy.bioimageanalysis.org/download	N/A
GraphPad Prism version 6.0	https://www.graphpad.com/	N/A
Other		
AB human serum Male HIV tested	Biowest	S4190-100
Hoechst 33342	Invitrogen	H3570
Protein G Sepharose 4 Fast Flow	GE healthcare	17-0618-01

LEAD CONTACT AND MATERIALS AVAILABILITY

Further information for resources and reagents should be directed to and will be provided by the Lead Contact, Jean-Luc Perfettini (perfettini@orange.fr).

EXPERIMENTAL MODEL AND SUBJECT DETAILS

Cell lines

The monocyte THP1 cells and CEM-SS T cells were maintained in RMPI-1640-Glutamax medium supplemented with 10% heat inactivated fetal bovine serum (FBS) and 100 UI/mL penicillin-streptomycin (Life technology). THP1 cells were obtained from ATCC. THP1 macrophages were obtained by treatment for 3 hours with 100 nM phorbol-12-myristate-13-acetate (PMA, Invivogen) of THP1 monocytes and after extensive washings were let to differentiate for 72 hours before experimentation. HeLa cells stably transfected with the Env gene of HIV-$1_{LAI/IIIB}$ (HeLa Env^+), HeLa cells transfected with CD4 (HeLa $CD4^+CXCR4^+$), HeLa TZM-bl and HEK293T cells were cultured in Dulbecco's modified Eagle's medium (DMEM)-Glutamax supplemented with 10% FBS and 100 UI/ml penicillin-streptomycin, in the absence or presence of the indicated concentrations of inhibitors. All cell lines used were mycoplasma-free.

Primary Cells

To generate Monocytes Derived Macrophages (MDMs) for HIV-1 infections with HIV-1_{BaL}, $CD14^+$ monocytes were isolated from peripheral blood mononuclear cells (PBMCs) by positive selection using anti-CD14 beads (Miltenyi Biotec). Buffy coats from healthy

donors were obtained from the French blood bank (Etablissement Français du Sang (EFS)). In accordance with French law, written informed consent to use the cells for clinical research was obtained from each donor. Purified monocytes were incubated in RMPI-1640-Glutamax medium supplemented with 100 UI/ml penicillin-streptomycin and with 10% FBS in the presence of 10 ng/ml recombinant human (rh) M-CSF (PeproTech). After 6 days of culture, adherent cells corresponding to the macrophages enriched fraction were harvested, washed and used for HIV-1_{BaL} infection experiments. For macrophage silencing and infections with HIV-1_{AD8}, monocytes were separated from PBMCs by adherence to the plastic, detached and cultured for 6 days in hydrophobic Teflon dishes (Lumox Duthsher) in macrophage medium (RPMI 1640 supplemented with 200 mM L-glutamine, 100 U of penicillin, 100 μg streptomycin, 10 mM HEPES, 10 mM sodium pyruvate, 50 μM β-mercaptoethanol, 1% minimum essential medium vitamins, 1% non-essential amino acids (Life technology)) supplemented with 15% of heat inactivated human serum AB (Life technology or Biowest). For experiments, MDMs were harvested and resuspended in macrophage medium containing 10% of FBS. MDMs obtained with this method are 91 to 96% $CD14^+$, they express: the differentiation markers (CD11b and CD71) and the M2 macrophage polarization markers (CD163 and CD206) (Allouch et al., 2013).

T cells were prepared from the monocyte depleted cell fraction of PBMCs. Peripheral blood lymphocytes (PBLs) were activated for 48 hours in fresh medium supplemented with 2.5 μg/ml PHA (Sigma-Aldrich) and 1 μg/ml rhIL-2 (PeproTech). PBLs were then washed and cultured in growth medium containing 1 μg/mL rhIL-2 for 24 hours before HIV-1 infections.

Non-Human primates

Adult cynomolgus macaques (*Macaca fascicularis*) (four males and three females) were imported from Mauritius and housed in the facilities of the ''Commissariat à l'Energie Atomique et aux Energies Alternatives'' (CEA, Fontenay-aux-Roses, France). The protocols employed were approved by the ethical committee of the CEA ''Comité d'Ethique en Experimentation Animale'' registered in the French Research Ministry under number 44. Samples from lymph nodes, ileum and colon tissues were obtained from *Macaca fascicularis* that have been infected at the age of 5 years old by intrarectal inoculation with a single dose of 50 50% animal infectious doses (AID_{50}) of SIV_{mac251}. Tissues were collected during animal necropsy (for SIV_{mac251}-infected animals, on days 701 to 738 after SIV infection) after sedation of the animals (ketamine chlorhydrate 10 mg/kg) followed by euthanasia (injection of sodium pentobarbital 180 mg/kg). Non-human primates (NHP, which includes *M. fascicularis*) were used at the CEA in accordance with French national regulation and under national veterinary inspectors (CEA Permit Number A 92-032-02). The CEA is in compliance with Standards for Human Care and Use of Laboratory of the Office for Laboratory Animal Welfare (OLAW, USA) under OLAW Assurance number #A5826-01. The use of NHP at CEA is also in accordance with recommendation of the European Directive (2010/63, recommendation N°9). Animals were housed in adjoining individual cages allowing social interactions, under controlled conditions of humidity, temperature and light (12-hour light/12-hour dark cycles). Water was available *ad libitum*. Animals were monitored and fed 1-2 times daily with commercial monkey chow and fruits by trained personnel. Macaques were provided with environmental enrichment including toys, novel foodstuffs and music under the supervision of the CEA Animal Welfare Body. The animals were used under the supervision of the veterinarians in charge of the animal facility. Experimental procedures were conducted after animal sedation with ketamine chlorydrate (Rhone-Merieux, Lyon, France, 10 mg/kg) as previously described (Dioszeghy et al., 2006).

Human autopsies

Human autopsies from axillary lymph nodes and frontal cortex were obtained in accordance with the Italian and EU legislations, after approval by the Institutional Review Board of the Lazzaro Spallanzani National Institute for Infectious Disease (Ethics Committee approval number 40/2006). Axillary lymph nodes and post-mortem frontal cortex sections were obtained from healthy (6 and 5, respectively) and HIV-1- infected individuals (6 and 11, respectively) (all men, mean age 36 years, the median values of HIV-1 viral load was 4.5 ± 0.6 $\log_{10}$ cp/ml and < 500 CD4 T cells/μl). Frontal cortex sections were obtained from patients with HIV-1-associated dementia.

METHODS DETAILS

Plasmids and transfections

NLRP3 coding sequence in the pUNO vector was purchased from Invivogen. The Flag-tagged NLRP3 full-length coding sequence was inserted in the 3xFlag-pcDNA3 and are a kind of gift from Gabriel Nunez (He et al., 2014). The sequence coding for P2Y2 (in the pEFGP-N1 vector) is gift from Laura Erb (Seye et al., 2004). Transient transfections of HeLa $CD4^+CXCR4^+$ cells ($2.4x10^5$) or HEK293T ($3x10^5$) cells with mammalian expression vectors (1-5 μg) were performed using Fugene transfection reagent (Promega), following the manufacturer's instructions. Western blot, immunoprecipitation analyses and experiences of HIV-1 infection or cell fusion were performed 24 hours after transfection. The transfection of pHIV-1_{AD8} and pHIV-1_{NL4-3} in HEK293T were performed 48 hours after transfection of pFlag-Luciferase or p3xFlag-NLRP3.

siRNA- and shRNA-mediated knockdowns

For HeLa $CD4^+CXCR4^+$ knockdown the small interfering RNAs (siRNAs) used against NLRP3 were purchased from Sigma and had the following sequences: NLRP3, siRNA-1, 5′-GGAUCAAACUACUCUGUGA-3′; siRNA-2, 5′-UGCAAGAUCUCUCAGCAAA-3′ and the corresponding control siRNA, 5′-UUCAAUAAAUUCUUGAGGU-3′. The siRNAs against CBL used for primary MDMs and

HEK293T cells are siGenome (Dharmacon) smart pool selected composed of a pool of four siRNAs having the following sequences for CBL (siRNA1, 5′-GGAGACACAUUUCGGAUUA-3′; siRNA2, 5′-GAUCUGACCUGCAAUGAUU-3′; siRNA3, 5′-GACAAUCCCUCA CAAUAAA-3′; siRNA4, 5′-CCAGAAAGCUUUGGUCAUU-3′). The siRNAs used as control with siGenome smart pool are a pool of four on target plus non-targeting siRNAs (Dharmacon). siRNAs transfection of HeLa $CD4^+CXCR4^+$ or HEK293T cells were performed with 20 nM siRNA using Oligofectamine (Invitrogen) according to the manufacturer's instructions. Western blot analyses and experiences of HIV-1 infections or cell fusions were performed 48 hours after siRNA transfection. For siRNA transfection of MDMs, the protocol was previously described (Allouch et al., 2013): MDMs were seeded ($0.5x10^6$ MDMs/0.5 ml/ well of 12-well plate in macrophages medium + 10% FBS) and let to be attached at 37°C for 2 hours prior siRNAs transfection. The siRNAs transfections were performed with the INTERFERin (Polyplus Transfection). Different amounts of siRNAs were pre-diluted in 1 mL of Opti-MEM in which 20 μL of INTERFERin were added and the transfection mix was let to incubate at room temperature for 10 minutes. The transfection mix (250 μl) was added to $0.5x10^6$ MDMs at the final concentrations of 50 nM of siRNAs against CBL. Equal amounts of the on target plus non-targeting siRNAs were added to the control MDMs. The MDMs were then incubated at 37°C for overnight. The medium was replaced with fresh macrophage medium supplemented with 10% FBS prior to the infections. At 72 hours post-CBL siRNA transfection MDMs were infected with $HIV\text{-}1_{AD8}$ (MOI of 1) for 6 hours, cell lysates were assayed for protein expression by western blot.

For short hairpin RNA (shRNA) lentiviral particles transduction, the pLKO.1 shRNA expression lentiviral vector coding for each targeted gene was purchased from Thermo Scientific. The shRNAs used in knockdown experiments had the following sequences for P2Y2 (shRNA1, 5′-ATGTTCCACCTGGCTGTGTCTGATGCACT-3′), for NLRP3 (shRNA1, 5′-TTCTTGAAGTGTTTCTAACGC-3′, shRNA2, 5′-AAACAGTAGAACAATTCCAGC-3′) and pLKO.1 empty vector control. Lentiviral vector particles were generated by cotransfection of three plasmids coding for the gag-pol HIV-1 genes (pCMV- HIV-1-GAG-POL), for the vector genome carrying shRNA of interest (pLKO.1 shRNA) and for the plasmid coding for an envelope of VSVG (pMDG-VSV-G). Co-transfection was performed in HEK293T cells using Fugene transfection reagent (Promega) according to the manufacturer's protocol. Two days after transfection, supernatants were filtered using 0.45-μm cellulose acetate filters (Sartorius stedim), aliquoted and frozen at −80°C. For transduction, lentivirus productions were added to the monocytic THP1 cell line ($4x10^6$) or into $CD4^+CXR4^+$ HeLa cells (10^6) and 24 hours after transduction the medium was replaced with fresh growth medium containing 1 μg/mL puromycin (Invivogen). MDMs, CEM-SS T Cells or THP1 cells ($1x10^6$) were transduced with 2 μg CAp24 of a pool of LKO.1 shNLRP3 (shRNA1 and shRNA2) for 48 hours before infections with $HIV\text{-}1_{NL4\text{-}3}$ or $HIV\text{-}1_{AD8}$ (MOI of 1).

Virus productions

To produce stocks of wild-type $HIV\text{-}1_{NL4\text{-}3}$ or $HIV\text{-}1_{AD8}$, HEK293T cells ($2x10^6$) were transfected with 20 μg of the corresponding proviral DNA ($pHIV\text{-}1_{NL4\text{-}3}$ or $pHIV\text{-}1_{AD8}$) and for Env-deleted VSV-G pseudotyped NL4-3 viruses ($pHIV\text{-}1_{NL4\text{-}3\Delta Env}$), HEK293T cells ($2x10^6$) cells were transfected with 4 μg of VSV-G expression vector (pVSV-G) and 16 μg of HIV-1 proviral DNA ($pHIV\text{-}1_{NL4\text{-}3\Delta Env}$) by the calcium phosphate method. After 12 hours, the transfection mixture was replaced with 8 mL of fresh growth medium. Then, 24 hours later, the media containing the first batch of virus was harvested and 8 mL of fresh growth medium was added to the cells for additional 24 hours. $HIV\text{-}1_{NDK}$ and $HIV\text{-}1_{BaL}$ were obtained after infection of activated PBLs and MDM with $HIV\text{-}1_{NDK}$ and $HIV\text{-}1_{BaL}$ viral stocks, respectively and harvesting the corresponding supernatants at three and six days after infections (Saïdi et al., 2008). $HIV\text{-}1_{AD8\text{-}Vpr\text{-}GFP}$ was obtained through the transfection of $3x10^6$ HEK293T cells with 10 μg $pHIV\text{-}1_{AD8}$ (NIH AIDS research reagents), 2.5 μg pGFP-Vpr expression vectors using Fugene (Promega) following manufacturer's instructions.

Upon collection, all virus-containing media was low-speed centrifuged, filtered through a 0.45 μm pore size filter (Sartorius stedim), to remove cell debris, treated with Benzonase (Novagen®) and stored in 1 mL aliquots at −80°C (Delelis et al., 2009; Perfettini et al., 2004, 2005). Viral stocks were standardized by quantification of CAp24 antigen in cell culture supernatants with an enzyme-linked immunoabsorbent assay (Perkin Elmer) and infection of TZM-bl cells (bearing the β-galactosidase gene under the control of HIV-1 LTR) with serial dilutions of the viral stocks followed by cell fixation and X-Gal staining. The multiplicity of infection (MOI) was determined at 48 hours of infection of TZM-bl based on the number of the positive X-Gal cells.

Viral infections

After 3 days of infection with $HIV\text{-}1_{NDK}$ (MOI of 1), PHA/IL-2–stimulated peripheral blood lymphocytes were cocultured with uninfected lymphoblasts or alone for 48 hours and analyzed by immunofluorescence for synapse formation. MDMs were infected with $HIV\text{-}1_{BaL}$ (with a MOI of 2) during 3 days for the analysis by Proximity Ligation Assay (PLA) (following manufacturer's instructions) and the intracellular CAp24 by FACS, as previously described (Séror et al., 2011), for MSU (100 μM) and LPS (10 ng/ml) treated cells. MDMs or PMA-THP1 macrophages infected with $HIV\text{-}1_{AD8}$ were pre-treated 18 hours with MSU (100 μM) and AR-C118925XX (100 μM) and infected during six hours with $HIV\text{-}1_{AD8}$ (MOI of 1) in the presence of the indicated drugs. The quantification of the LDH release in the cell supernatants of MSU-treated MDM was performed using the commercially available ELISA kits for LDH (Roche) according to the manufacturers' instructions at 24 hours after infection.

THP1 cells were also infected with $HIV\text{-}1_{NL4\text{-}3}$ (MOI of 1) or $HIV\text{-}1_{NL4\text{-}3\Delta Env}$ (MOI of 1) during 6 hours and analyzed for related signaling pathways by western blot. THP1 monocytes or CEM-SS T cells were infected or not for 3 hours with X4-tropic $HIV\text{-}1_{NL4\text{-}3}$ or R5-tropic $HIV\text{-}1_{AD8}$ (MOI of 1) and then were either harvest for western blot and mRNA analysis or kept for 21 days by passing cells every 3 days for the same analysis.

For THP1 monocytes or CEM-SS T cells silenced for NLRP3, through the transduction of lentiviral vectors expressing shRNA1 and shRNA2 against NLRP3 gene, and control cells were infected with HIV-1_{NL4-3} or HIV-1_{AD8} (MOI of 1) at 48 hours after shRNA transduction for 6 hours and after washings were suspended in equal medium volumes. Cell supernatants were then harvested at 6 and 12 days after infection for quantification of HIV-1 CAp24 contents. For immunoprecipitation assays, THP1 cells were treated 8 hours with PP1 (20 μM), PP2 (20 μM) or 2 hours of pretreatment with UTP (100 μM) before infection. Then, THP1 cells were infected during 6 hours with HIV-1_{NL4-3} (MOI of 1) in the presence of the indicated drugs. To remove the membrane bound non-internalized HIV-1 particles before analysis of intracellular CAp24 by western blot, cells were treated with trypsin at 37°C for 20 minutes followed by two extensive washings. Target cell infectivity was evaluated using the enhanced β-galactosidase assay kit (Roche). PMA-THP1 macrophages were infected with HIV-$1_{AD8\text{-}Vpr\text{-}GFP}$ (MOI of 1) in the presence of latrunculin B (10 μM) during 6 hours and the control cells were treated with ethanol and then were fixed with 2% PFA for immunofluorescence analysis.

Immunofluorescence

Cells were fixed in 2% paraformaldehyde-PBS for 5 minutes, permeabilized in 0.3% Triton (Sigma) in PBS or 0.1% Triton for MDMs and PBLs, and incubated with PBS-FBS 20% for 1 hour. Tissue 4-μm sections (lymph nodes, ileum and colon tissues) were cut from the paraffin blocks of the paraformaldehyde fixed tissues from *Macaca fascicularis* or humans. After paraffin removal, slides were subjected to antigen retrieval by microwave boiling in 1 mmol/l EDTA pH 9.0. Cell slides were then incubated during overnight for immunofluorescence with anti-P2Y2 (Alomone), anti-NLRP3 (Adipogen), anti-CD163 (BD laboratories) or anti-gp120 (2G12) (AIDS Research and Reference Reagent Program, Division of AIDS, NIAID) or for immunochemistry with anti-NLRP3 (Sigma) after permeabilization in 0.3% Triton for 5 minutes and saturation in PBS-FBS 20% for 1 hour. Then, cells were incubated with appropriate secondary antibodies conjugated to Alexa Fluor 488, 546 or 647 fluorochromes (Life technologies) at room temperature during 1 hour and 30 minutes. Actin was stained with Alexa Fluor 594 Phalloidin for 30 minutes at room temperature. DNA was stained with Hoechst 33342, Trihydrochloride, Trihydrate (Life technologies) and then cells were mounted with Flouromount G medium (Southern biotech). Proximity Ligation Assay (DUOLINK®, Sigma) was performed according to the manufacturer's instructions using anti-NLRP3 (Adipogen) and anti P2Y2 (Alomone) as primary antibodies. Images of cells were acquired by laser-scanning fluorescent confocal microscopy Leica SPE with LAS-X software (Leica) with 8 bits configuration and using a 63X oil objective (1.4 numerical aperture). Leica Microsystem immersion oil (11513859) was used and imaging was performed at room temperature. Confocal images were analyzed with ImageJ and exported as TIFs for figures illustration. For 3D immunofluorescence intensity image construction, images were analyzed by Icy software (in Figure 1G).

Western blots and immunoprecipitations

Cells were washed twice with PBS and lysed in appropriated buffer (250 mM NaCl, 0.1% NP-40, 5 mM EDTA, 10 mM Na3VO4, 10 mM NaF, 5 mM DTT, 3 mM Na4P2O7, 1 mM EGTA, 10 mM Glycerol phosphate, 10 mM Tris-Hcl (pH = 7.5) and the protease and phosphatase inhibitors (Roche)). 10-40 μg of protein extracts were run on 4%–12% or 10% SDS-PAGE and transferred at 4°C onto a nitrocellulose membrane (0.2 Micron). After incubation for 2 hours at room temperature with 5% nonfat milk or BSA (Bovine Serum Albumin) in Tris-buffered saline and 0.1% Tween 20 (TBS-Tween), membranes were incubated with primary antibody at 4°C overnight. Horseradish peroxidase–conjugated goat anti–mouse or anti–rabbit (SouthernBiotech) antibodies were then incubated for 1 hour 30 minutes and revealed with the enhanced ECL detection system (GE Healthcare) in the linear range. The primary antibodies for western blot against CBL (D4E10), GFP (D5.1), PYK2 (5E2), PYK2Y402*, SRC (36D10) and SRCY416* were obtained from Cell Signaling. Primary antibodies against ACTIN and GAPDH were purchased from Abcam and Millipore, respectively. The primary antibodies anti-CAp24 (42-50) and anti-gp120 (2G12) were from NIH (AIDS Research and Reference Reagent Program, Division of AIDS, NIAID). Antibody anti-NLRP3 was from Adipogen (Cryo-2), anti-P2Y2 was from Alomone, anti-ubiquitin (UB) (P4D1) was from Santa-Cruz, and anti-Flag was from Sigma. For immunoprecipitations, cell pellets were lysed at indicated times after infection or 24 hours after transfection in CHAPS buffer (50 mM Tris- HCl (pH = 7.5), 0.50 M NaCl and 0.1% CHAPS) containing protease and phosphatase inhibitors. Anti-P2Y2 (Alomone) antibodies were incubated overnight at 4°C with 500 μg cell lysates. The complexes were precipitated by incubation with Protein G Sepharose 4 Fast Flow (GE Healthcare) for 4 hours. For relative expression quantification analyzed protein bands were quantified by ImageJ software and normalized on the corresponding endogenous expression of GAPDH or ACTIN proteins. To determine the relative NLRP3 interacting with P2Y2, NLRP3 protein bands were normalized on the corresponding immunoprecipitated P2Y2.

Flow cytometry

For flow cytometry, THP1 cells and MDMs (10^6 cells/ml) were harvested in RPMI complete medium, washed twice with PBS, saturated at 4°C for 20 min with PBS-FBS 10% and incubated with anti-CD4 (FITC) and anti-CD184 (CXCR4) (PE-Cy5) antibodies. The indicated antibodies and isotype-matched antibodies used were obtained from BD PharMingen. Phenotypic analyses on primary human MDMs infected by HIV-1_{BaL} were realized by flow cytometry using mAb anti-CD163 (FITC) (BioLegend), anti-CD206 (Alexa Fluor®647 (AbD Serotec) and anti-p24 (PE) (Beckman Coulter).

Quantitative PCR (qPCR)

The quantification of the HIV-1 early reverse transcripts (ERT) was based on the quantification of HIV-1 R-U5 DNA and performed as previously described (David et al., 2006). DNA was extracted with the DNeasy Tissue Kit (QIAGEN) at 24 h.p.i for ERT detection in MDMs. The quantitative PCR analysis was carried on an ABI prism 7000 Sequence Detection System. The amounts of HIV-1 cDNA copies were normalized to the endogenous reference gene albumin. Standard curve were generated by serial dilutions of a commercial human genomic DNA (Roche).

For the detection of NLRP3 mRNA, total RNA from $0.25x20^6$ THP1 monocytes or CEM-SS T cells were extracted using RNeasy kit (QIAGEN). RNA was transcribed using SuperScript II RT (Invitrogen). The predesigned Applied Biosystems probes for NLRP3 gene (Hs00918082 m1) and GAPDH (Hs02758991 g1) (for normalization) were used. These probes were included in the premade TaqMan Gene expression mixes obtained from thermofisher scientific. The results were analyzed with the cycle threshold method (CT) and each sample was normalized to the quantity of endogenous GAPDH mRNA.

QUANTIFICATION AND STATISTICAL ANALYSIS

Statistical parameters including exact values of n, precisions measures (mean ± SEM), statistical significances and the tests used for each analysis are reported in the Figures and Figures legends. All values were expressed as the mean ± SEM of cell individual samples. Samples values were analyzed using two-tailed unpaired Student's t test for two groups, ANOVA for multiple comparisons groups, Mann-Whitney test for human MDMs and PBLs donors not normalized data and Wilcoxon signed rank test for MDMs donors analyzed for early reverse transcripts. Significance levels are * $p \leq 0.05$, ** $p \leq 0.01$, *** $p \leq 0.001$ and **** $p \leq 0.0001$. Statistical analysis was performed in GraphPad Prism version 6.0b (GraphPad Software). No statistical test was used to determine sample size. No samples were excluded for analysis. The experiments were not randomized. Investigators were not blinded to allocation during experiments and outcome assessments.

DATA AND CODE AVAILABILITY

The western blot data reported in this paper have been deposited on Mendeley Data (Mendeley data https://doi.org/10.17632/6bxgc4h4m2.1) and are accessible to readers upon request.